

1 **GTDI: a gaming integrated drought index implying hazard**
2 **causing and bearing impacts changing**

3 Xiaowei Zhao¹, Tianzeng Yang¹, Hongbo Zhang^{1,2,3*}, Tian Lan¹, Chaowei Xue¹, Tongfang Li¹, Zhaoxia
4 Ye¹, Zhifang Yang¹, Yurou Zhang¹

5

6 ¹ School of Water and Environment, Chang'an University, Xi'an, 710054, China

7 ² Key Laboratory of Subsurface Hydrology and Ecological Effect in Arid Region of Ministry of
8 Education, Chang'an University, Xi'an, 710054, China

9 ³ Key Laboratory of Eco-hydrology and Water Security in Arid and Semi-arid Regions of the
10 Ministry of Water Resources, Chang'an University, Xi'an 710054, China

11

12 **Abstract:** Developing an effective and reliable integrated drought index is crucial for tracking and
13 identifying droughts. The study employs game theory to create a spatially variable weight drought
14 index (GTDI) by combining two single-type indices: the agricultural drought index (SSMI), which
15 implies drought hazard-bearing conditions, and the meteorological drought index (SPEI), which
16 implies drought hazard-causing conditions. Also, the entropy theory-based drought index (ETDI) is
17 induced to incorporate a spatial comparison to the GTDI to illustrate the rationality of gaming weight
18 integration. Leaf Area Index (LAI) data is employed to confirm the reliability of the GTDI in
19 identifying drought by comparing it with the SPEI, SSMI, and ETDI. Furthermore, ~~an assessment~~ [a](#)
20 [comparative analysis](#) is conducted on the temporal trajectories and spatial evolution of the GTDI-
21 identified drought to discuss the GTDI's advancedness in monitoring changes in hazard-causing and

22 bearing impacts. [Also, the entropy theory-based drought index \(ETDI\) is induced to incorporate a](#)
23 [spatial comparison to the GTDI to illustrate the rationality of gaming weight integration, as both](#)
24 [entropy theory and game theory belong to linear combination methods in the development of the](#)
25 [integrated drought index, and entropy theory has been applied in related research.](#) The results
26 showed that the GTDI has a greatly high correlation with single-type drought indices (SPEI and
27 SSMI), and its gaming weight integration is more logical and trustworthy than the ETDI. As a result,
28 it outperforms ETDI, SPEI, and SSMI in recognizing drought spatiotemporally, and is projected to
29 replace single-type drought indices to provide a more accurate picture of actual drought.
30 Additionally, GTDI exhibits the gaming feature, indicating a distinct benefit in monitoring changes
31 in hazard-causing and bearing impacts. The case studies show drought events in the Wei River Basin
32 are dominated by a lack of precipitation. The hazard-causing index SPEI dominates the early stages
33 of a drought event, whereas the hazard-bearing index SSMI dominates the later stages. This study
34 surely serves as a helpful reference for the development of integrated drought indices as well as
35 regional drought ~~mitigation~~, prevention, ~~—~~ and monitoring.

36
37 **Keywords:** Integrated drought index; GTDI; drought identification; LAI; Wei River Basin

38 **1 Introduction**

39 Drought is one of the most widespread and frequent natural hazards, commonly associated with
40 inadequate rainfall, a deficit in soil moisture, and reduced stream flow (Berg et al., 2018; Zhang et
41 al., 2022; AghaKouchak et al., 2023). Due to the combined pressures of climate change and human
42 activities, the intensity of global drought and the area of arid land have expanded dramatically since

43 the 21st century (Dai et al., 2013; Huang et al., 2016), severely constraining socio-economic
44 development and human livelihoods. Moreover, global warming is projected to increase the
45 frequency and severity of future drought occurrences (Trenberth et al., 2014; Vicente-Serrano et al.,
46 2020).

47 China, with its complex terrain and diverse climate types, is one of the countries suffering the
48 most severe drought-related losses worldwide (Dai et al., 2011; Zhang et al., 2021). Drought is
49 responsible for more than half of the economic losses caused by climatic hazards in China (Wang et
50 al., 2023). According to the Ministry of Water Resources of China (MWRC, 2022), the average
51 annual impacted area of crops and grain loss due to drought was 19.51 million hm² and 15.8 billion
52 kg, respectively, from 1950 to 2022. The loss has become increasingly severe, particularly after
53 2006, resulting in direct economic losses of more than US\$ 160 billion in China. For example, the
54 severe drought event that occurred in southern China from autumn 2009 to spring 2010 deprived
55 almost 21 million people of drinking water, with direct economic losses of nearly US\$3 billion
56 (Yang et al., 2012). Furthermore, the ongoing drought in China may worsen in the future (Leng et
57 al., 2015; Wang et al., 2018), with drought-occurrences becoming more frequent, intense, and
58 extended. As a result, scientifically identifying regional drought risks and clarifying regional
59 drought development and evolution patterns can assist in actively developing drought mitigation
60 and disaster reduction strategies, assuring the security of food supply and water use.

61 Drought is currently categorized into four types based on distinct description objects:
62 meteorological, agricultural, hydrological, and socioeconomic droughts (Wilhite and Glantz, 1985;
63 Shah and Mishra, 2020). ~~Meteorological drought is characterized by insufficient precipitation,~~
64 ~~whereas agricultural drought occurs when soil moisture fails to meet crop development requirements.~~

65 ~~Hydrological drought is primarily caused by a lack of surface runoff and groundwater (Xu et al.,~~
66 ~~2019; Saha et al., 2023). Socioeconomic drought arises when the aforementioned causes disrupt the~~
67 ~~human socioeconomic system, resulting in an imbalance between water supply and demand (Ding~~
68 ~~et al., 2021).~~ Despite differing definitions and emphasis, meteorological drought is always regarded
69 as the root cause of the other three types of drought (Ma et al., 2020). In terms of the driving
70 mechanism of drought occurrences, meteorological drought indicates the causative attribute of
71 drought (Zhang et al., 2023), whereas the other three primarily reflect the state of hazard-bearing
72 entities. Concurrently examining the hazard-causing and hazard-bearing components of drought is
73 essential for effective estimation and management of drought risk.

74 Drought is frequently identified using drought indices. The Standardized Precipitation Index
75 (SPI; Mckee et al., 1993) for meteorological drought, the Standardized Soil Moisture Index (SSMI;
76 Hao and AghaKouchak, 2013) for agricultural drought, and the Standardized Runoff Index (SRI;
77 Shukla and Wood, 2008) for hydrological drought are currently the most commonly used drought
78 indices. These single-type drought indices are primarily used for one-dimensional (type) drought
79 measurement & evaluation. However, due to the ~~complexity and diversity~~ complex causes and wide-
80 ranging impacts of drought events, a single-type drought index ~~is unavoidably insufficient to handle~~
81 ~~the complete drought development process~~ usually cannot fully and effectively reflect the
82 spatiotemporal development process of drought events (Chang et al., 2016; Wei et al., 2023). As a
83 result, much effort has been expended in developing comprehensive drought indices, such as the
84 Palmer Drought Severity Index (PDSI; Palmer, 1965). However, these indices are not very
85 successful at distinguishing between meteorological and agricultural drought influences and
86 evaluating changes in regional patterns. Because of this, some works refer to constructing a

87 composite or integrated drought index in two or more dimensions (Chang et al., 2016; Won et al.,
88 2020; Wei et al., 2023), employing both linear and nonlinear combination approaches.

89 The copula function is commonly employed in the nonlinear approach. Won et al. (2020)
90 proposed a copula-based joint drought index (CJDI) by combining the SPI and the evaporative
91 demand drought index (EDDI); Wei et al. (2023) used the copula function to connect precipitation,
92 NDVI, and runoff and then constructed the standardized comprehensive drought index (SCDI),
93 which ~~has had~~ been applied to drought assessment in China's Yangtze River Basin. It should be
94 noted that copula functions are ~~heavily~~ possibly reliant on the assumption that samples follow a
95 specific probability density function (Zhang et al., 2019). However, due to the complicated
96 interactions between the atmosphere, vegetation, soil, and groundwater, the drought does not
97 generally meet it. If the copula function is used to estimate drought quantiles, significant biases may
98 be introduced, affecting the reliability of the copula-based integrated drought indices (Huang et al.,
99 2015).

100 ~~An comprehensive-~~ integrated drought index can also be generated by linearly mixing single-
101 type drought indices, such as the entropy weight method (Huang et al., 2015) and the principal
102 component analysis method (Liu et al., 2019). In the relevant research, it is highly emphasized that
103 the weighting of different types of drought indices is critical since it has a significant impact on the
104 reliability of drought monitoring results (Liu et al., 2019; Wei et al., 2023). Furthermore, it has been
105 revealed that the impacts of different factors on drought ([Blauhut et al., 2016](#); [Zhang et al., 2022](#)),
106 such as hazard-causing and hazard-bearing, are changing spatially and game-playing, necessitating
107 the development of effective linear combination methods for measuring their spatial heterogeneity
108 in contribution to drought. Therefore, game theory is suggested for the integration of drought indices

109 because it can comprehensively consider the opinions of each party to achieve a distribution pattern
110 that satisfies each participant (Lai et al., 2015; Jato-Espino and Ruiz-Puente, 2021), [which is](#)
111 [superior to the entropy weight method in weight allocation, and its calculation process is simpler](#)
112 [than copula functions.](#) ~~and~~ It has been widely applied in water resources management (Madani, 2010;
113 Khorshidi et al., 2019; Batabyal and Beladi, 2021).

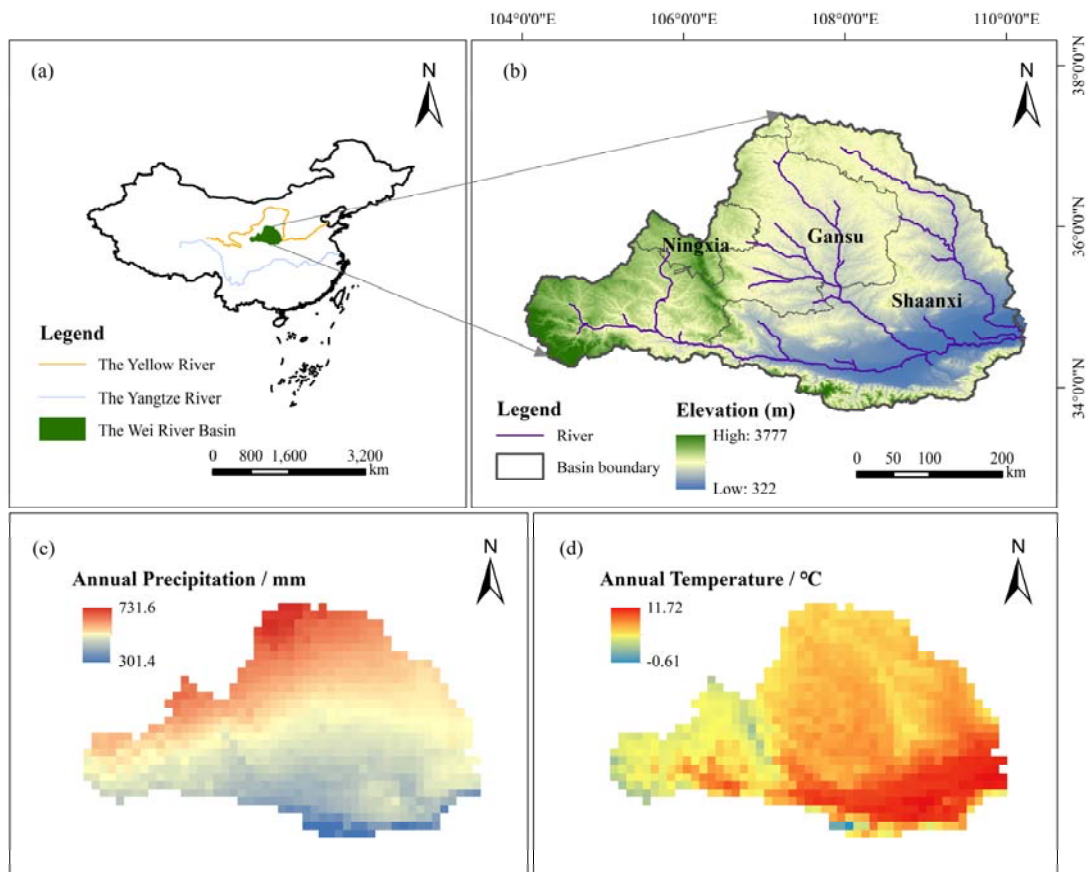
114 This study proposes a game theory-based drought index (GTDI), which integrates the
115 meteorological drought index SPEI, implying hazard-causing impact, and the agricultural drought
116 index SSMI, implying hazard-bearing impact, through the game theory method. The structure of
117 this study is as follows: Section 2 introduces the research topic and data source. Section 3 describes
118 the SPEI, SSMI, GTDI, and ETDI (entropy theory-based drought index) calculation procedures, as
119 well as the verification and analysis methodologies. Section 4 investigates the evolutionary features
120 of GTDI, examines its rationality of integrated weight in comparison to ETDI, and validates its
121 usefulness in identifying drought occurrences using Leaf Area Index (LAI) data. Furthermore, the
122 impact of hazard-causing and bearing indices on GTDI's spatiotemporal evolution is explored
123 through the synergistic analysis of GTDI, SPEI, and SSMI. Finally, Section 5 highlights the study's
124 significant findings.

125 **2 Study area and data**

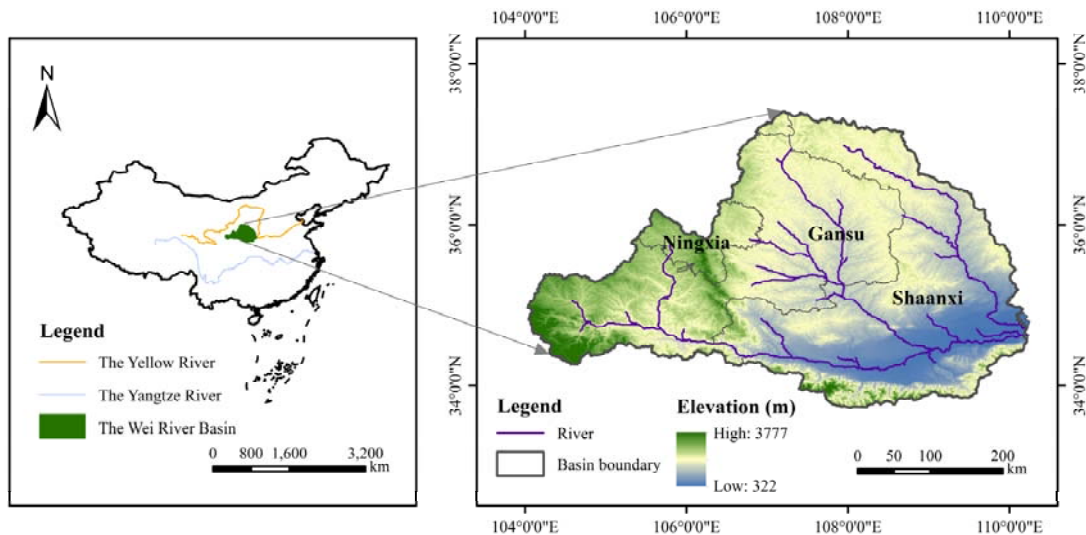
126 **2.1 Study area**

127 The Wei River is the largest tributary of the Yellow River, with a drainage area of 134,800 km² (Fig.
128 1). It rises to the north of Niaoshu Mountain in Gansu Province, about 33.5°–37.5°N latitude and
129 103.5°–110.5°E longitude, and runs primarily through Shaanxi, Gansu, and Ningxia provinces. The

130 Wei River Basin (WRB) is high in the west and low in the east, with a geographical elevation ranging
131 from 322 to 3777 meters. The WRB has a continental monsoon climate with large seasonal
132 fluctuations, with average annual temperatures and precipitation ranging from 7.8 to 13.5°C and
133 500 to 800 mm, respectively (Zhang et al., 2022). Precipitation in the WRB accounts for over 60%
134 of the total annual amount, and its spatial distribution shows a steady decrease from southeast to
135 northwest. Furthermore, evaporation is significant in the WRB, with annual water surface
136 evaporation ranging from 660 to 1600 mm. As a result of its specific climate characteristics, the
137 WRB is a typical place for drought research.



138



139

140 **Figure 1.** A map of the Wei River Basin.

141 **2.2 Data source**

142 The data used in this study comprises: (1) DEM data with a grid size of 30 m; (2) monthly
 143 precipitation and temperature dataset ([Peng et al., 2019](#)) from 1950 to 2020 with a grid size of 1 km;
 144 (3) GLDAS_NOAH025_3H_2.0 and GLDAS_NOAH025_3H_2.1's soil moisture dataset for 0 to
 145 10 cm of soil surface layer, with a spatial resolution of 0.25° and data period from 1950 to 2020; (4)
 146 GLOBMAP leaf area index dataset (Version 3) with a period of 1981 to 2019 and a spatial resolution
 147 of 0.08° ([Liu et al., 2012](#)). Additionally, in order to facilitate calculation and analysis, precipitation,
 148 air temperature, soil moisture, and leaf area index (LAI) data were all resampled to the same spatial
 149 resolution of 0.125° [using the bilinear interpolation method](#) in this study. The data source is shown
 150 in Table 1.

151 **Table 1.** Data source.

Name	Source
DEM data	http://www.ncdc.ac.cn/
Precipitation dataset	http://www.geodata.cn/
Temperature dataset	http://www.geodata.cn/
Soil moisture dataset	https://disc.gsfc.nasa.gov/datasets/

152 **3 Methodology**

153 **3.1 Calculation of single-type drought indices**

154 **3.1.1 SPEI**

155 The Standardized Precipitation Evapotranspiration Index (SPEI) was first introduced by Vicente
156 Serrano et al. in 2010. As a meteorological drought index, SPEI primarily characterizes the hazard-
157 causing attribute of drought (Zhang et al., 2023). On the basis of the Standardized Precipitation
158 Index (SPI), SPEI takes potential evapotranspiration (PET) into account and demonstrates superior
159 effectiveness and applicability (Labudová et al., 2017; Li et al., 2020; Tan et al., 2023). The
160 Thornthwaite method, which can better reflect the potential surface evapotranspiration, is employed
161 to calculate PET in this paper. As is well known, drought indices on different time scales can reflect
162 the dry and wet conditions of the study area during different periods. [The 3-month drought index](#)
163 [can reflect short- and medium-term dry and wet conditions and is more sensitive to seasonal drought,](#)
164 [which helps us identify and analyze seasonal drought in the Wei River Basin.](#) ~~In this study~~ Therefore,
165 we calculated the SPEI series over a three-month timescale [in this study](#). The detailed calculation
166 ~~procedure~~ [method of the SPEI for SPEI](#) can be found in ~~Vicente Serrano et al. (2010)~~ [Supplement](#)
167 [S1](#).

168 **3.1.2 SSMI**

169 Drought can have a direct impact on the growth state of hazard-bearing bodies such as crops (Zhang
170 et al., 2023), making agricultural drought hazard-bearing. The Standardized Soil Moisture Index

171 (SSMI) is one of the most effective indices for predicting agricultural drought (Hao et al., 2013),
172 and its calculation method is comparable to that of the SPI (Xu et al., 2021; You et al., 2022).
173 Meanwhile, it was revealed that the log-logistic probability distribution function with three
174 parameters was better suited to soil moisture data ~~sequences~~ series than the original gamma
175 probability distribution function (Oertel et al., 2018). As a result, in this study, we employed the
176 calculation method proposed by Oertel et al. for the agricultural drought index SSMI, with a three-
177 month time scale, just like the SPEI. And the calculation method of the SSMI is detailed in
178 Supplement S2. ~~As a result, in this study, we employed the calculation method proposed by Oertel~~
179 ~~et al. for the agricultural drought index SSMI, with a three-month time scale, just like the SPEI.~~

180 **3.2 Construction of integrated drought indices**

181 In this study, two integrated drought indices, the GTDI and ETDI, are built utilizing game theory
182 and the entropy weight method for index weight allocation, respectively, and both combine the SPEI
183 and SSMI. The ETDI serves as a comparison to the GTDI in this study, and Supplement S3
184 introduces the calculation process of the ETDI. ~~Huang et al. (2015) provide the computation process~~
185 ~~for it.~~

186 As a subset of optimality modeling, game theory (GT) investigates the interacting outcomes of
187 resource conflicts and cooperation between two or more entities (Lai et al., 2015). It attempts an
188 optimal allocation approach that maximizes the interests of each participant through mathematical
189 analysis (Jato-Espino and Ruiz-Puente, 2021). Currently, GT has been widely applied in the fields
190 of hydrology and water resources, such as water price equilibrium (Batabyal and Beladi, 2021),
191 reservoir scheduling policy (Khorshidi et al., 2019), and subjective/objective weighting issues (Liu

192 et al., 2020). In this study, the hazard-causing index (SPEI) and the hazard-bearing index (SSMI)
 193 are regarded as two opponents in the game. Through confrontation, the GT technique gets the ideal
 194 weight allocation for both sides and then uses this to produce the integrated drought index (GTDI)
 195 at each grid point. The following are the methods for creating GTDI using game theory:

196 **Step 1:** A possible weight set is combined by SPEI and SSMI in the form of an arbitrary linear
 197 combination as follows:

$$V = \alpha_{spei} V_{spei}^T + \alpha_{ssmi} V_{ssmi}^T, (\alpha_{spei}, \alpha_{ssmi} > 0) \quad (1)$$

198 ~~Where~~ where V is a possible combined vector, V_{spei} & V_{ssmi} are the weight vectors of SPEI and SSMI,
 199 and α_{spei} & α_{ssmi} are the weight coefficients.

200 **Step 2:** Minimize the deviation between V and V_k using the following formula:

$$\text{Min} \|V - V_k\|_2, (k = spei, ssmi) \quad (2)$$

201 **Step 3:** According to the differentiation property of the matrix, transform formula (2) into a
 202 first-order system of linear equations:

$$\begin{bmatrix} V_{spei} V_{spei}^T & V_{spei} V_{ssmi}^T \\ V_{ssmi} V_{spei}^T & V_{ssmi} V_{ssmi}^T \end{bmatrix} \begin{bmatrix} \alpha_{spei} \\ \alpha_{ssmi} \end{bmatrix} = \begin{bmatrix} V_{spei} V_{spei}^T \\ V_{ssmi} V_{ssmi}^T \end{bmatrix} \quad (3)$$

203 **Step 4:** Solve the weight coefficients α_{spei} and α_{ssmi} in equation (3) and normalize them.

$$\begin{cases} \alpha_{spei}^* = \alpha_{spei} / (\alpha_{spei} + \alpha_{ssmi}) \\ \alpha_{ssmi}^* = \alpha_{ssmi} / (\alpha_{spei} + \alpha_{ssmi}) \end{cases} \quad (4)$$

204 **Step 5:** Calculate GTDI:

$$V_{gtdi} = \alpha_{spei}^* V_{spei}^T + \alpha_{ssmi}^* V_{ssmi}^T \quad (5)$$

205 ~~Where~~ where V_{gtdi} is the combined vector of GTDI, α_{spei}^* and α_{ssmi}^* are the normalized weight
 206 coefficients of SPEI and SSMI, respectively.

207 3.3 Classification criteria for drought

208 **Table 2.** Drought classification criteria for the SPEI, SSMI, GTDI and ETDI ([Huang et al., 2023](#)).

Grade	Classification	Values
1	No drought	-0.5 < Index
2	Mild drought	-1.0 < Index ≤ -0.5
3	Moderate drought	-1.5 < Index ≤ -1.50
4	Severe drought	-2.0 < Index ≤ -1.5
5	Extreme drought	Index ≤ -2.0

209 The calculating approach of SSMI in this study is comparable to that of SPEI, while GTDI and
 210 ETDI are built on SSMI and SPEI. As a result, as indicated in Table 2, the SSMI, GTDI, and ETDI
 211 use the same grading criteria as the SPEI.

212 3.4 Reliability verification

213 3.4.1 Evaluation of correlation

214 A correlation analysis of the integrated drought index with two single-type drought indices is
 215 necessary to assess the consistency of indicators before and after coupling. Thus, the Pearson's
 216 correlation coefficients (PCC) ([Panda et al., 2018](#)) between GTDI/ETDI with SPEI and SSMI are
 217 calculated for each grid (Eq. 6), and their correlation in different locations is explored. Table 3 shows
 218 the correlation levels and corresponding absolute value range of PCC.

$$PCC_{x,y} = \frac{\sum_{i=1}^n (x_i - \bar{x})(y_i - \bar{y})}{\sqrt{\sum_{i=1}^n (x_i - \bar{x})^2 \sum_{i=1}^n (y_i - \bar{y})^2}} \quad (6)$$

219 ~~Where~~ where n denotes the sample size; x_i and y_i are data samples of x and y , respectively; \bar{x} and
 220 \bar{y} are arithmetic average of x and y , respectively.

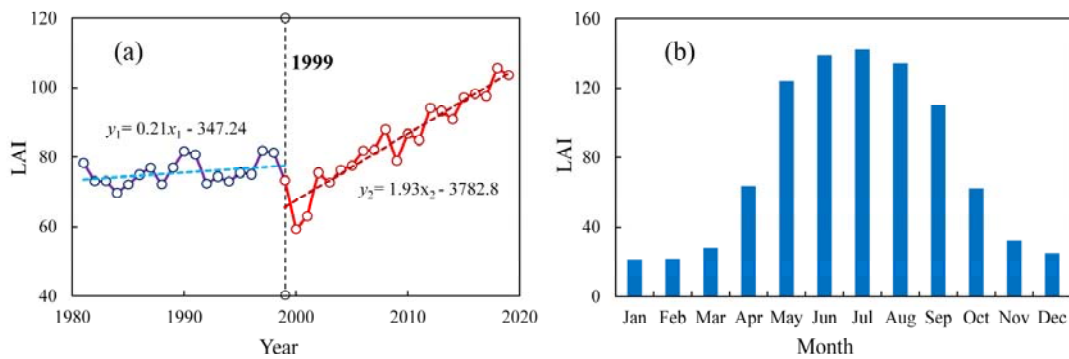
221 **Table 3.** The absolute value range of PCC and correlation levels ([Yang and He, 2022](#)).

Correlation levels	Absolute values of PCC
--------------------	------------------------

Greatly low or none	[0, 0.2]
Low	(0.2, 0.4]
Moderate	(0.4, 0.6]
High	(0.6, 0.8]
Greatly high	(0.8, 1.0]

222 3.4.2 Efficacy verification in identifying drought

223 Because surface vegetation is highly sensitive to soil moisture (Li et al., 2022), drought usually leads
 224 to a decrease in vegetation Leaf Area Index (LAI; Fang et al., 2019; Bock et al., 2023). In light of
 225 this, LAI data are used to evaluate the drought recognition capabilities of various ~~indexes~~ indices to
 226 further validate their dependability. The leaf area index dataset used is the GLOBMAP leaf area
 227 index product (<https://www.resdc.cn/>).



228
 229 **Figure 2.** The plot graphs of the Leaf Area Index (LAI) in the Wei River Basin with an interannual
 230 trend spanning from 1981 to 2019 (a) and the average monthly allocation from 1981 to 1999 (b).

231 Significant disparities in LAI trends can be identified in the WRB around 1999, as illustrated
 232 in Fig. 2(a). Prior to 1999, the average annual growth rate of LAI was only 0.21/a, but it skyrocketed
 233 to 1.93/a after 1999, owing mostly to "Grain for Green" (Li et al., 2019; Tian et al., 2022). In order
 234 to mitigate the potential inaccuracy resulting from the regional LAI trend change, we selected the
 235 validation years of 1981 to 1999, during which the growth trend was relatively weak. Also, LAI in
 236 the WRB rises significantly from March to August, falls fast from September to November, and then

237 remains low from December to January of the following year (Fig. 2b). It can be discovered that
 238 LAI's trend change in autumn and winter is the result of vegetation's natural growth cycle, resulting
 239 in a reduced sensitivity of LAI to soil moisture and further failing to identify drought. As a result,
 240 the autumn and winter months (September to January) should also be excluded from the validation
 241 period.

242 In summary, LAI raster data from March to August (spring and summer) of the period from
 243 1981 to 1999 were selected to verify the drought identification efficacy of drought indices.
 244 Meanwhile, the image from the mid-month of each month is regarded as the representative data of
 245 the month. If the occurrence of drought has been discovered, it can be determined by comparing the
 246 mean values of the LAI ~~drought index values~~ during arid months with non-arid months. The specific
 247 process is as follows:

$$\begin{cases} M_{d,i} = \frac{\sum_{j=1}^m I_{i,j}}{m} \\ M_{n,i} = \frac{\sum_{l=1}^n I_{i,l}}{n} \end{cases} \quad (7)$$

$$R_i = \begin{cases} 1, M_{d,i} < M_{n,i} \\ 0, M_{d,i} \geq M_{n,i} \end{cases} \quad (8)$$

248 ~~Where~~ where $M_{d,i}$ and $M_{n,i}$ represent the average values of the ~~drought index~~ LAI in the i -th grid
 249 during arid and non-arid months, respectively; m and n are the number of arid and non-arid months,
 250 respectively; $I_{i,j}$ and $I_{i,l}$ represent the ~~drought index~~ value of the LAI of the i -th grid during the j -th
 251 arid month and the l -th non-arid month, respectively; R_i represents the drought recognition
 252 performance of the drought index in the i -th grid, with a value of 1 indicating fine and 0 indicating
 253 poor.

254 **3.5 Analysis methods for drought characteristics**

255 **3.5.1 Mann-Kendall test**

256 The Mann-Kendall (M-K) test is a non-parametric statistical test method with a simple
257 computational process ([Yue and Wang, 2002](#)). It has been extensively utilized for the analysis of
258 hydrological and meteorological sequences (Zhang et al., 2021; Agbo et al., 2023). In this study, the
259 M-K test method is used to perform trend testing on the drought index sequences, and the calculation
260 principle can be referred to Cai et al. (2022).

261 **3.5.2 Drought identification**

262 Drought is often identified by two factors: the drought index threshold and the drought area
263 threshold. In this study, we used -1 as the drought index threshold, which is compatible with current
264 research (Deng et al., 2021; Feng et al., 2023), and 1.6% as the area threshold (Wang et al., 2011).
265 Furthermore, a spatiotemporal continuity technique is used to detect drought occurrences, with
266 specific procedures available in Deng et al. (2021). Briefly, as long as the drought index value at a
267 grid point is lower than the drought index threshold of -1, we determine it as a drought grid point.
268 When the total area of drought grid points in a certain month exceeds the drought area threshold,
269 we determine that month as a drought month. Furthermore, when multiple consecutive months are
270 determined to be drought months, if the overlapping area of drought areas in space between two
271 adjacent consecutive drought months exceeds the drought area threshold, we determine that these
272 two months belong to the same drought event, otherwise, they belong to different drought events.

273 3.5.3 Spatiotemporal characteristics of drought

274 The spatiotemporal characteristics of drought mostly manifest in variables such as drought intensity,
 275 drought area, drought duration, and drought centroid (Wen et al., 2020). Based on the current
 276 research methods for studying the spatiotemporal characteristics of drought, we divided the
 277 variables representing drought characteristics into two scales: grid point and monthly, in order to
 278 systematically analyze and describe the drought characteristics of the WRB.

279 (1) Grid point's drought characteristic variable

280 The drought intensity S_i of the grid point is calculated by:

$$S_i = S_0 - I_i \quad (9)$$

281 ~~Where~~ where I_i is the value of the i -th drought grid point; S_0 is the threshold of the drought index.

282 (2) Monthly drought characteristic variables

283 The monthly drought characteristic variables consist of the monthly drought intensity S_{am} , the
 284 monthly drought area A_{am} , and the monthly drought centroid (X_{am}, Y_{am}) , as shown in Table 4.

285 **Table 4.** Monthly drought characteristic variables.

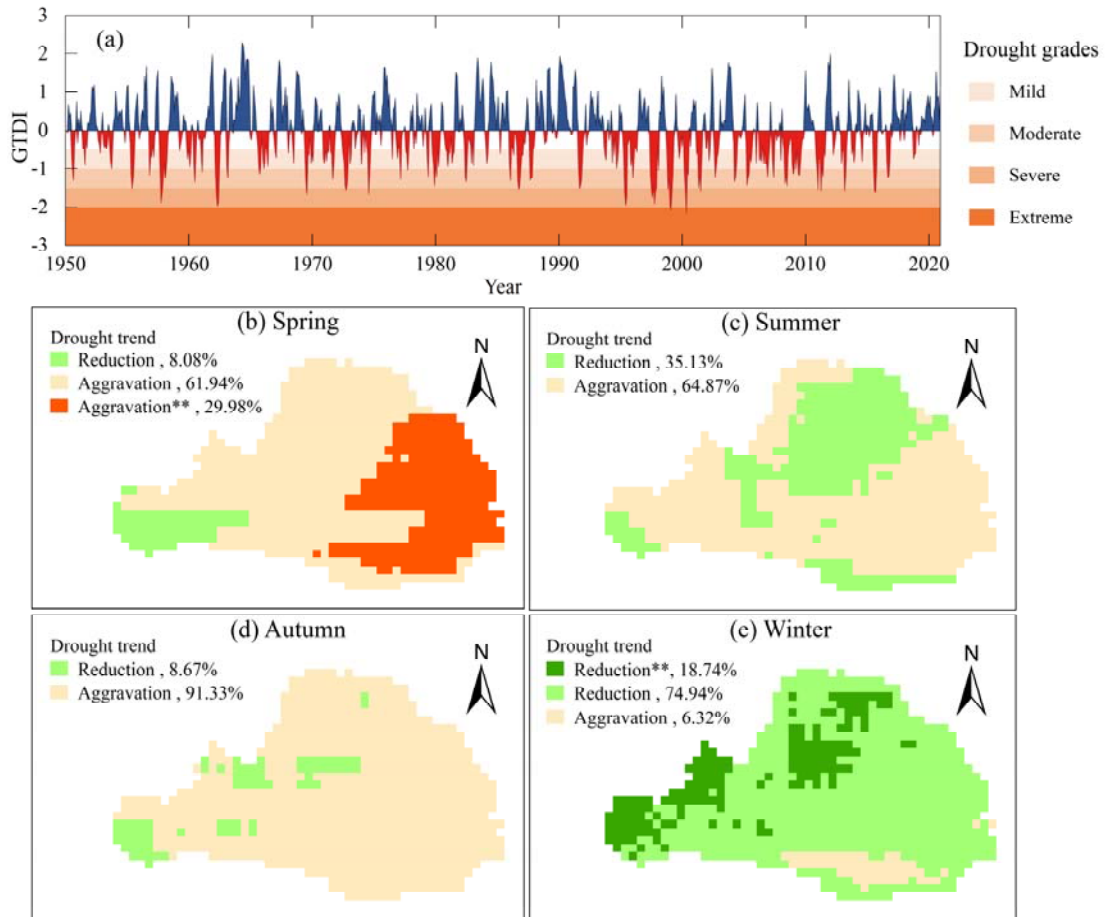
Variables	Formula	Notes	Number
Monthly drought intensity S_{am}	$S_{am} = \frac{1}{k} \sum_{i=1}^k S_i$	Where k is the number of drought grids; S_i is the intensity value of the i -th drought grid.	(10)
Monthly drought area $A_{am}/10^4\text{km}^2$	$A_{am} = kA$	Where A is the spatial range of a single grid, and its unit is 10^4 km^2 .	(11)
Monthly drought centroid (X_{am}, Y_{am})	$\begin{cases} X_{am} = \sum_{i=1}^k S_i x_i / \sum_{i=1}^k S_i \\ Y_{am} = \sum_{i=1}^k S_i y_i / \sum_{i=1}^k S_i \end{cases}$	Where S_i is the drought intensity value of the i -th drought grid, and x_i and y_i are the longitude and latitude coordinates of the i -th drought grid, respectively.	(12)

286 **4 Results and Discussion**

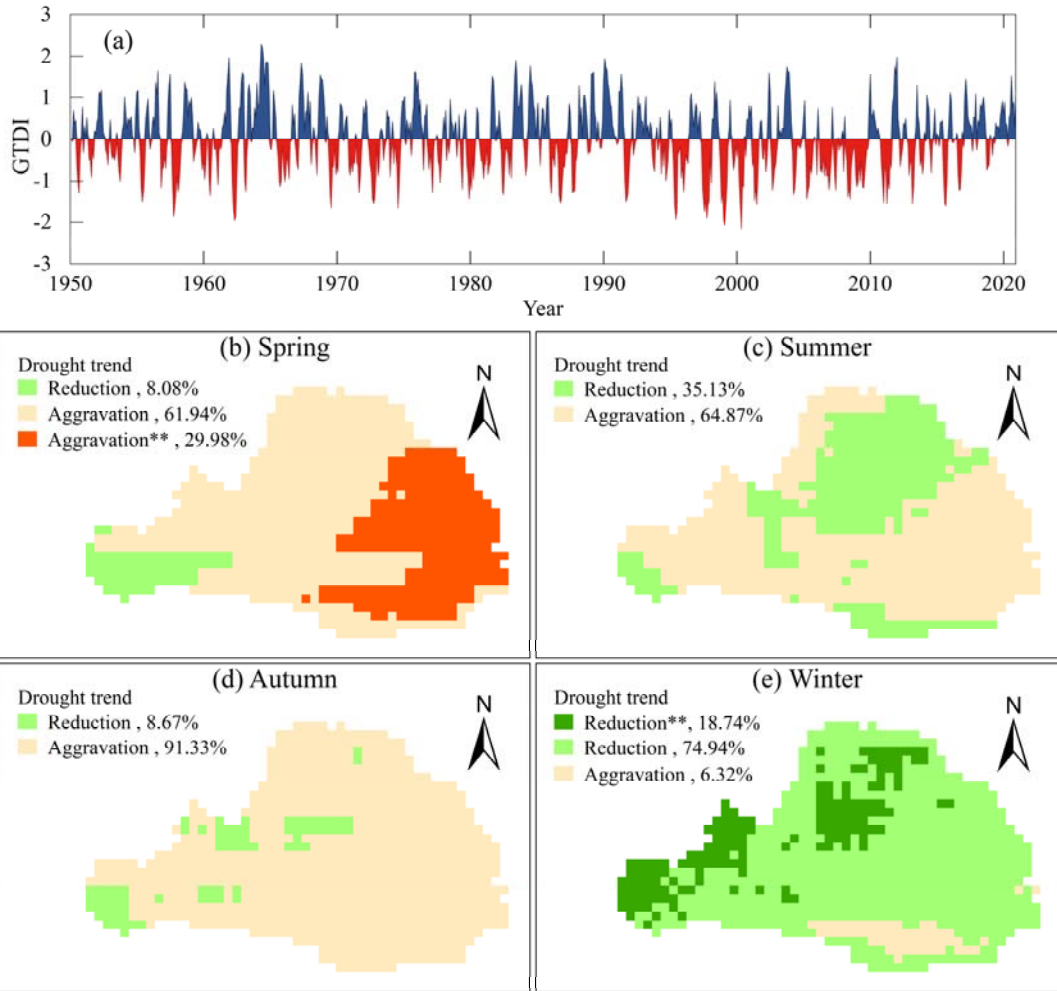
287 **4.1 Evolutionary characteristics of integrated drought index GTDI**

288 Using the game theory method, the monthly GTDI of the WRB was calculated based on SPEI and
289 SSMI. Meanwhile, considering the WRB's seasonal characteristics, GTDI sequences from May,
290 August, November, and February of the next year were chosen to represent the drought conditions
291 of spring, summer, autumn, and winter, respectively.

292 Fig. 3(a) demonstrates the temporal evolution characteristics of the monthly GTDI in the WRB
293 from 1950 to 2020. Therein, the linear tendency rate of GTDI is $-0.024/10a$, illustrating that the
294 drought in the WRB is aggravating, which is also mentioned in Wang et al. (2020). Particularly since
295 the 1990s, the frequency of moderate and severe drought months and their average drought intensity
296 have increased by 5.1% (from 34.1% to 39.2%) and 0.043 (from 0.242 to 0.285), respectively. In
297 terms of seasonal change, drought in the WRB showed an increasing trend in spring, summer, and
298 autumn (Fig. 3b-d). In the eastern half of the WRB, the significantly aggravated area of spring
299 drought accounts for 29.98% of the overall basin, while most places in summer and autumn show a
300 non-significant aggravation in drought severity. Winter is an exception, as most areas experience a
301 reduction in drought, especially in the eastern and northern regions of the WRB (Fig. 3e).



302



303

304 **Figure 3.** Temporal evolution characteristics of integrated drought in the Wei River Basin from 1950
 305 to 2020 (a), and spatial distribution of drought trends in different seasons (b-e). The symbol “***”
 306 donates the change is significant, and the percentage means the area proportion of different trend
 307 types.

308 4.2 Reliability verification of the GTDI

309 4.2.1 The evaluation of correlation

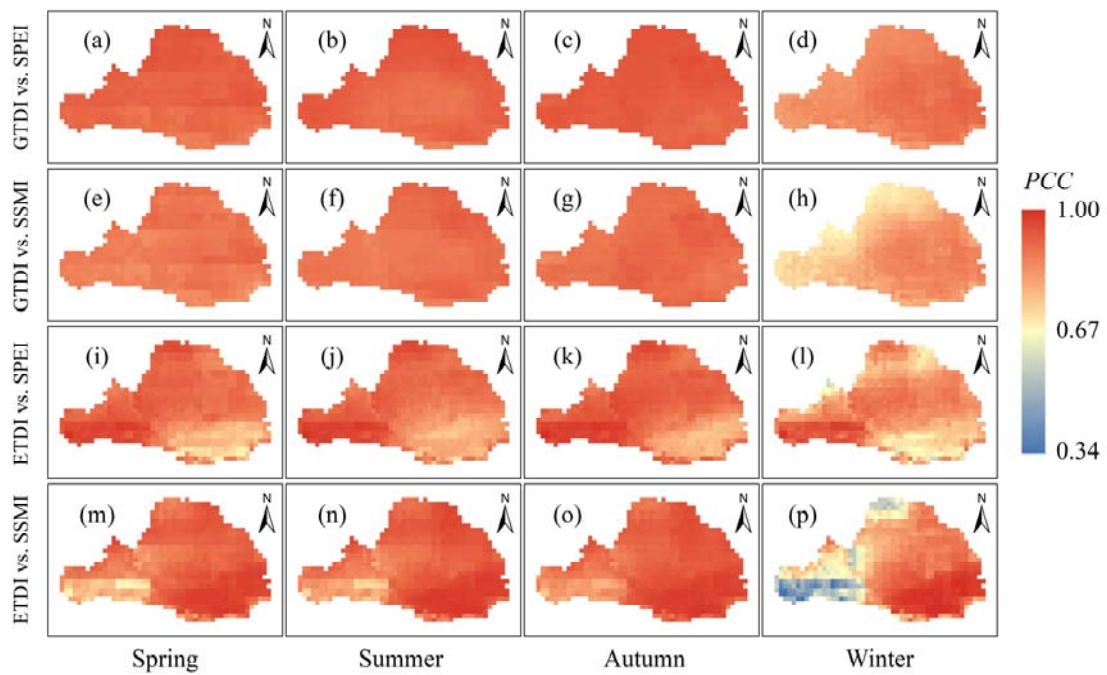
310 Table 5 illustrates the grid proportions of different correlation levels between the integrated drought
 311 indices (GTDI and ETDI) and the single-type drought indices (SPEI and SSMI), whereas Fig. 5

312 depicts the spatial distribution of their correlation coefficients in different seasons.

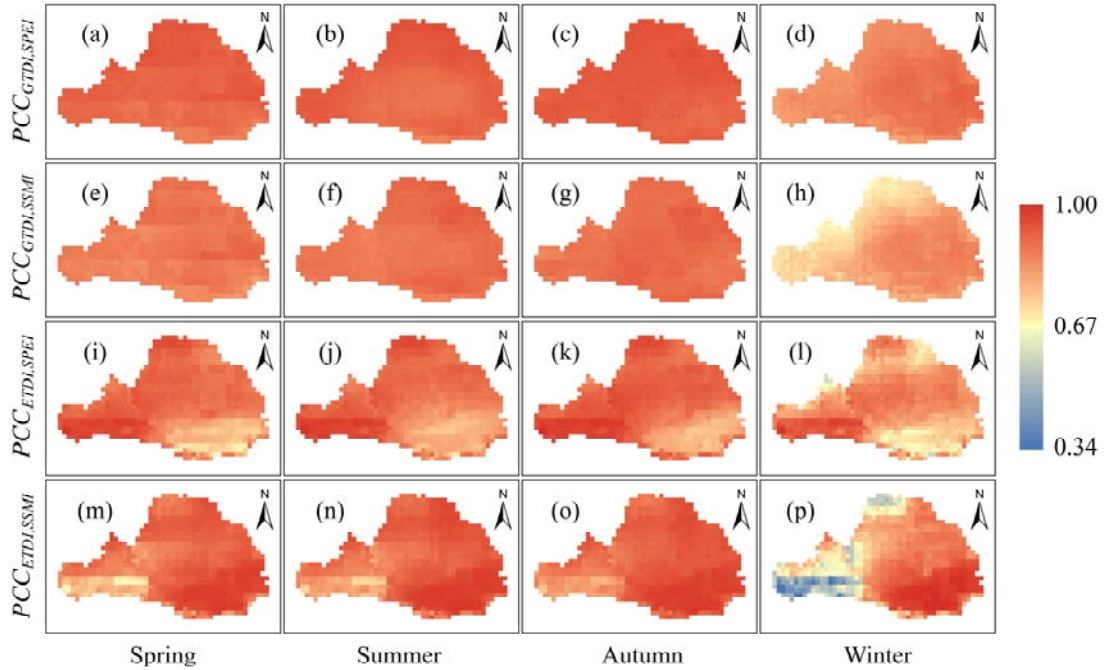
313 **Table 5.** Grid proportions of integrated drought indices (GTDI, ETDI) and single-type drought
 314 indices (SPEI, SSMI) at different correlation levels.

Correlation levels	GTDI vs. SPEI				GTDI vs. SSMI			
	Spring	Summer	Autumn	Winter	Spring	Summer	Autumn	Winter
Greatly high	100%	100%	100%	100%	100%	100%	100%	54.8%
High	0	0	0	0	0	0	0	45.2%

Correlation levels	ETDI vs. SPEI				ETDI vs. SSMI			
	Spring	Summer	Autumn	Winter	Spring	Summer	Autumn	Winter
Greatly high	83.6%	89.5%	88.4%	66.2%	89.7%	95.6%	98.2%	68.3%
High	16.4%	10.5%	11.6%	33.3%	10.3%	4.4%	1.8%	25.8%
Moderate	0	0	0	0.5%	0	0	0	5.4%
Low	0	0	0	0	0	0	0	0.5%



315



316

317 **Figure 4.** Spatial distribution of correlation coefficients in different seasons. The color bar on the
 318 right denotes the [Pearson's](#) correlation coefficients.

319

320

321

322

323

324

325

326

327

328

329

330

As shown in Table 5 and Fig. 4, the correlation between GTDI and SPEI or SSMI in the entire WRB is quite significant, and the correlation coefficients (PCC) are close to 1 in spring, summer, and autumn, but slightly ~~worse~~-lower in winter (Fig. 4a-h). The correlation coefficients in the western and northern areas of the WRB are lower in winter (Fig. 4d, h, l, p), but the minimal correlation coefficients between GTDI and SPEI or SSMI are still above 0.83 and 0.67, respectively (Fig. 4d, h). It is worth noting that GTDI and SPEI have a greatly high correlation across the WRB over all four seasons, whereas 45.2% of locations only have a good correlation between GTDI and SSMI in winter (Table 5). As a result, the correlation between GTDI and SPEI is stronger than that of SSMI, especially during the winter season.

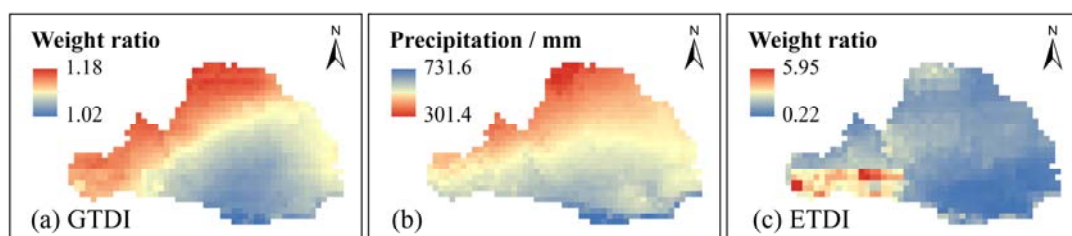
The graph also shows that the integrated drought index (ETDI) demonstrates spatially opposite correlations with SPEI and SSMI. For instance, in the southeastern area of the Wei River Basin, there is the worst association between ETDI and SPEI, but the correlation between ETDI and SSMI

331 is the strongest (Fig. 4i-p). Similar to GTDI, the correlation between ETDI and SPEI or SSMI is
 332 slightly higher in spring, summer, and autumn than in winter. However, as compared to GTDI, the
 333 geographical variability of the correlation coefficients between ETDI and SPEI or SSMI is more
 334 pronounced in the same season (Fig. 4). As seen in winter (Fig. 4p), the highest correlation
 335 coefficient between ETDI and SSMI is approximately 1, while the lowest value is around 0.34. In
 336 terms of grid proportions at various levels of correlation, the correlations between ETDI and SPEI
 337 or SSMI do not achieve a greatly high level in certain regions over the four seasons (Table 5),
 338 resulting in ~~their~~ its performance falling short compared to GTDI.

339 Overall, GTDI exhibits superior performance to ETDI, particularly in terms of the homogeneity
 340 of the spatial distribution of correlation coefficients, indicating that the integrated drought index
 341 GTDI constructed in this study has more reliable consistency with single-type drought indices (SPEI
 342 and SSMI).

343 4.2.2 Comparison of the integrated weight of GTDI and ETDI

344 To contrast the weight allocation ~~distribution~~ of SPEI and SSMI in creating the integrated drought
 345 indices GTDI and ETDI, the spatial distribution of their weight ratios (SPEI/SSMI) in the WRB is
 346 plotted, as shown in Fig. 5.



347
 348 **Figure 5.** Comparison of the integrated weights of GTDI and ETDI. Subfigures (a) and (c)
 349 demonstrate the spatial distribution of weight ratio (SPEI/SSMI) in the construction process of

350 GTDI and ETDI, respectively, and (b) is a spatial distribution map of the average annual
351 precipitation in the Wei River Basin.

352 The GTDI, an ~~comprehensive-integrated~~ drought index constructed using the game theory
353 method, exhibits a spatial distribution of the weight ratio (SPEI/SSMI) that gradually decreases from
354 northwest to southeast (Fig. 5a). Furthermore, the weight ratio in GTDI ranges from 1.02 to 1.18,
355 showing a substantially balanced weight allocation between the hazard-causing index (SPEI) and
356 the hazard-bearing index (SSMI). Meanwhile, the weight ratio of SPEI to SSMI is closer to 1 in
357 places with greater precipitation (Fig. 5a-b). It is noteworthy that the change in weight ratio
358 (SPEI/SSMI) in GTDI closely resembles the spatial distribution pattern of the average annual
359 precipitation in the WRB, as evidenced by a correlation coefficient of -0.88, indicating a significant
360 negative relationship.

361 The entropy theory-based drought index (ETDI), on the other hand, does not show a distinct
362 spatial distribution pattern for the weight ratio of SPEI to SSMI. Its weight ratio fluctuates greatly
363 between locations, ranging from 0.22 to 5.95 (Fig. 5c), implying that entropy theory fails to establish
364 a consistently stable allocation of weights in the integrated drought index ETDI development
365 process. Furthermore, the weight ratio (SPEI/SSMI) in ETDI has a low relationship with annual
366 average precipitation, as evidenced by a correlation coefficient of only -0.04.

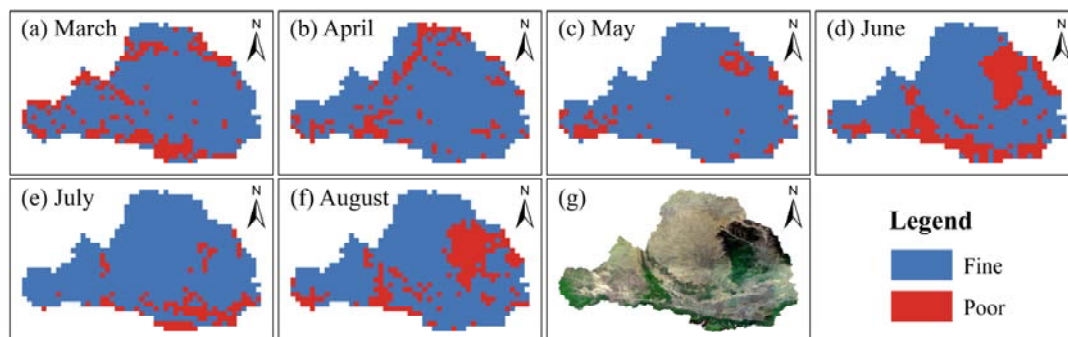
367 As a consequence of comparing GTDI and ETDI, it ~~is~~-was discovered that the game theory
368 approach gives an integrated weight geographic distribution compatible with the precipitation-
369 dominated natural drought pattern, which is essentially congruent with the drought generation
370 mechanism in this basin. As a result, it is thought that the weighting of SPEI and SSMI in GTDI is
371 more reasonable and reliable.

372 **4.2.3 The efficacy verification in identifying drought**

373 To further investigate the reliability of the integrated drought index GTDI, the Leaf Area Index (LAI)
 374 data is used to assess its efficacy in identifying drought, and the drought recognition performance
 375 of the GTDI is evaluated by Eq. 8 and presented in Fig. 6. To compare, Fig. 7 depicts the spatial
 376 distribution of efficacy in recognizing drought using the ETDI, SPEI, and SSMI, and Table 6
 377 provides a statistical list exhibiting the efficacy ratios of four drought indices in different validation
 378 months.

379 **Table 6.** The efficacy ratios of four drought indices in different validation months

Drought indices	March	April	May	June	July	August
GTDI	78.6%	84.1%	90.4%	71.8%	87.5%	76.3%
ETDI	48.4%	49.6%	50.7%	50.5%	49.2%	48.6%
SPEI	50.1%	49.5%	50.6%	49.4%	48.4%	48.8%
SSMI	49.1%	50.4%	52.8%	49.9%	49.5%	48.9%

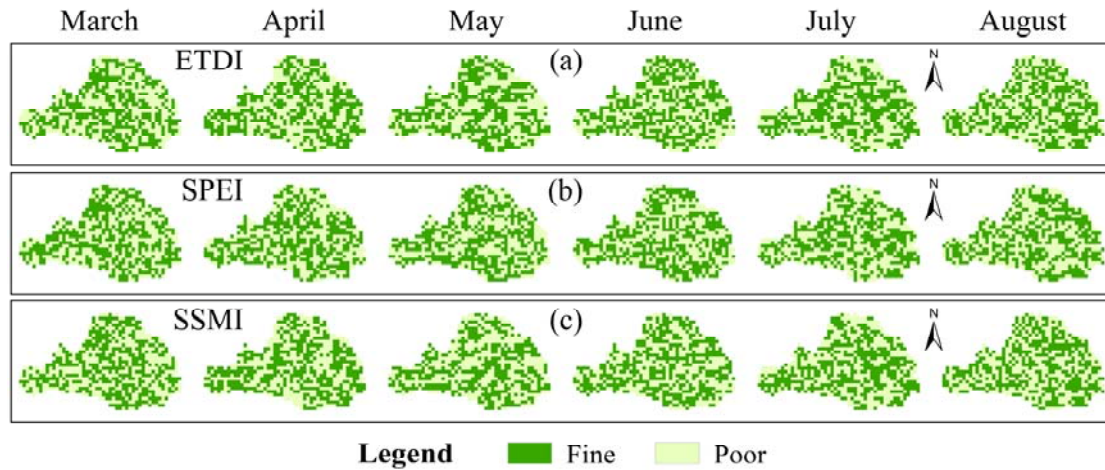


380
 381 **Figure 6.** The spatial distribution of GTDI's efficacy in identifying drought in the Wei River Basin.

382 Subfigures (a)-(f) depict the findings from March to August, and (g) displays a satellite image of the

383 Wei River Basin. ["Fine" means that the drought index accurately captured the occurrence of drought.](#)

384 [while "Poor" means that the drought index did not capture the occurrence of drought.](#)



385

386 **Figure 7.** The spatial distribution of efficacy in identifying drought of the ETDI, SPEI and SSMI.

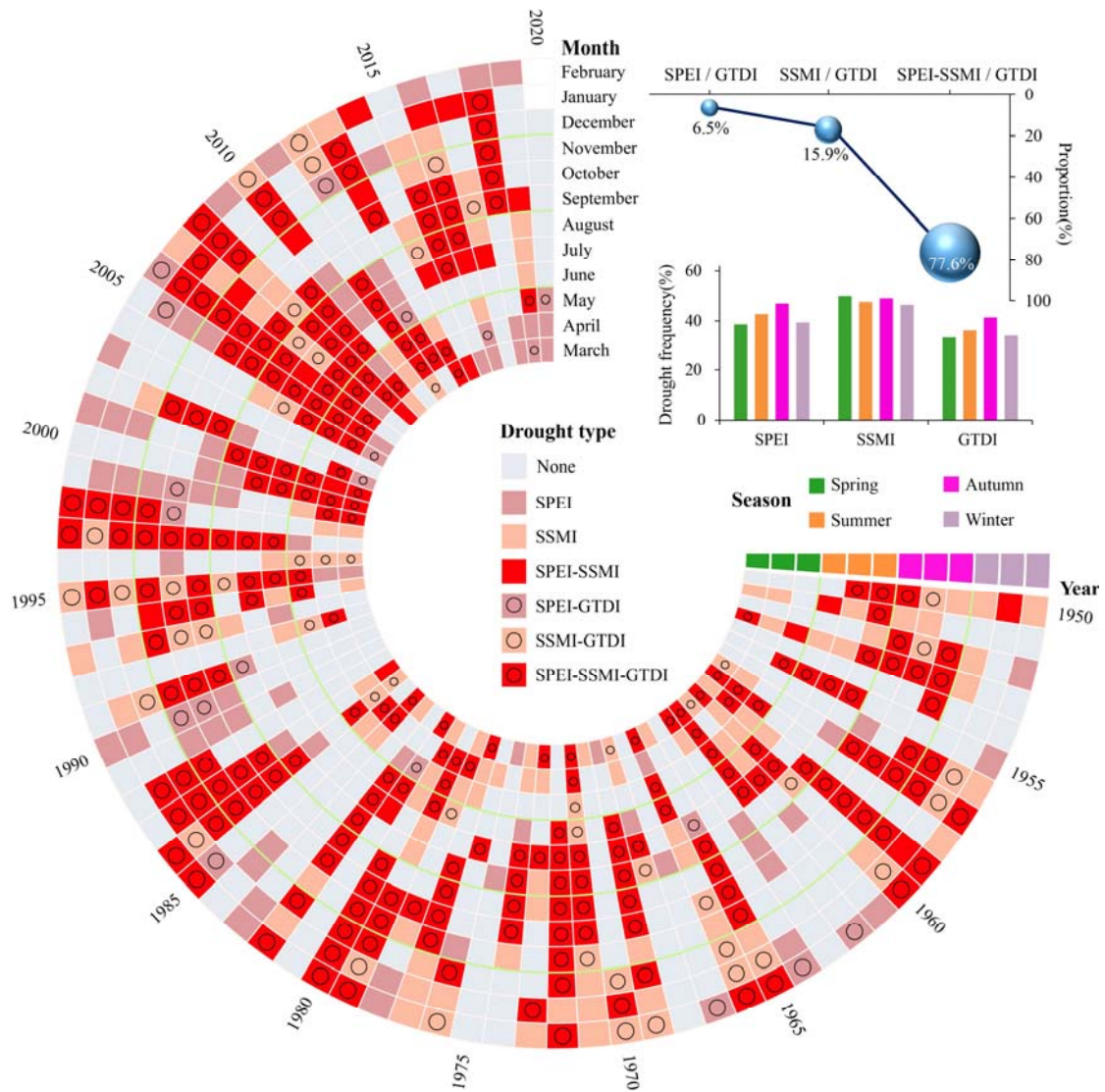
387 During the validation period from March to August, GTDI performs well in recognizing
 388 drought (Fig. 6), particularly in May, when it captures 90.28% of the drought in the WRB (Table 6).
 389 GTDI, on the other hand, performs relatively badly in June (Fig. 6d) and August (Fig. 6f), only with
 390 71.8% and 76.3% of effective recognition grid points, respectively (Table 6). In conjunction with
 391 Fig. 6(g), it is discovered that the grid points with poor performance in June and August are
 392 concentrated in the forest area, which is the dark green area in the WRB's northeast hinterland. As
 393 is widely known, forests have more access to deeper soil moisture than farming land and grassland
 394 (Xu et al., 2018; Bai et al., 2023), resulting in forests having higher drought tolerance than other
 395 terrestrial vegetation types (Jiang et al., 2020; Chen et al., 2022). However, the soil moisture data
 396 used in this study ~~is~~ are only 0 to 10cm of soil surface layer, which could explain why GTDI's
 397 drought diagnosis ability in the forest region is skewed. Even with the defect in forest regions, GTDI
 398 has exhibited strong drought monitoring capabilities in the WRB, and can effectively capture the
 399 occurrence of drought.

400 In contrast to GTDI, the effectiveness of drought detection by ETDI, SPEI, and SSMI is
 401 geographically random and chaotic, as illustrated in Fig. 7. Furthermore, in all validation months,

402 ETDI, SPEI, and SSMI only provide efficacy ratios of around 50%, indicating a lack of significant
403 usefulness in identifying drought (Table 6). As a result, when compared to ETDI, SPEI, and SSMI,
404 it is clear that GTDI provides significant advantages in the field of drought monitoring. To
405 summarize, GTDI does not simply combine the hazard-causing index (SPEI) and the hazard-bearing
406 index (SSMI) as ETDI, but it can indeed capture drought occurrence in most areas, addressing the
407 issue of single-type drought indices' insufficient responsiveness to actual drought events.

408 **4.3 Comparison of temporal trajectories of drought identified by** 409 **GTDI, SPEI, and SSMI**

410 The drought identification trajectories of the integrated drought index (GTDI), single-type drought
411 indices (SPEI and SSMI) during the study period are depicted in Fig. 8. Out of the 850 months
412 spanning from March 1950 to December 2020, merely 345 months are devoid of any drought,
413 accounting for approximately 40.6% of the total, which contradicts our common understanding of
414 drought incidents. Among the 505 dry months, 409 months experience agricultural drought (SSMI,
415 48.1%), 356 months experience meteorological drought (SPEI, 41.9%), and 260 months (30.6%)
416 experience both simultaneously. GTDI identifies just 308 arid months (36.2%) out of 850 months,
417 which is lower than SSMI and SPEI. According to the data presented above, agricultural drought
418 has been the most common occurrence in the WRB over the last 70 years, followed by
419 meteorological drought, with GTDI identifying the fewest number of drought months.



420

421 **Figure 8.** Comparison of the SPEI, SSMI and GTDI in temporal drought trajectories. "SPEI-SSMI"
 422 means that it is recognized as a drought month by SPEI and SSMI simultaneously, and the meanings
 423 of other drought types are similar to that.

424 Out of the GTDI-identified drought months, the proportion of meteorological drought
 425 occurring alone is 6.5%, and the proportion of agricultural drought occurring alone is 15.9%,
 426 possibly due to high temperatures, while the proportion of meteorological drought and agricultural
 427 drought occurring simultaneously is up to 77.6%. Thus, it is clear that GTDI is closely related to the
 428 hazard-causing index (SPEI) and the hazard-bearing index (SSMI) and is caused by both in most
 429 cases. It corresponds to the general public's understanding of drought incidents. Furthermore,

430 because it is calculated by weighting SPEI and SSMI, GTDI has an advantage in depicting the
431 temporal gaming evolution of SPEI and SSMI. From the perspective of seasonal distribution,
432 meteorological drought occurs most commonly in the summer and autumn, with a frequency of
433 more than 40%, but less frequently in the winter and spring. At the same time, agricultural drought
434 (SSMI) occurs at a frequency of over 45% in all seasons, with a very similar frequency in four
435 seasons. The seasonal allocation mode of drought identified by GTDI is similar to that of SPEI, with
436 the similarity being that it occurs more frequently in summer and autumn than in winter and spring.
437 However, the frequency of drought determined by SPEI is slightly higher than that determined by
438 GTDI in each season.

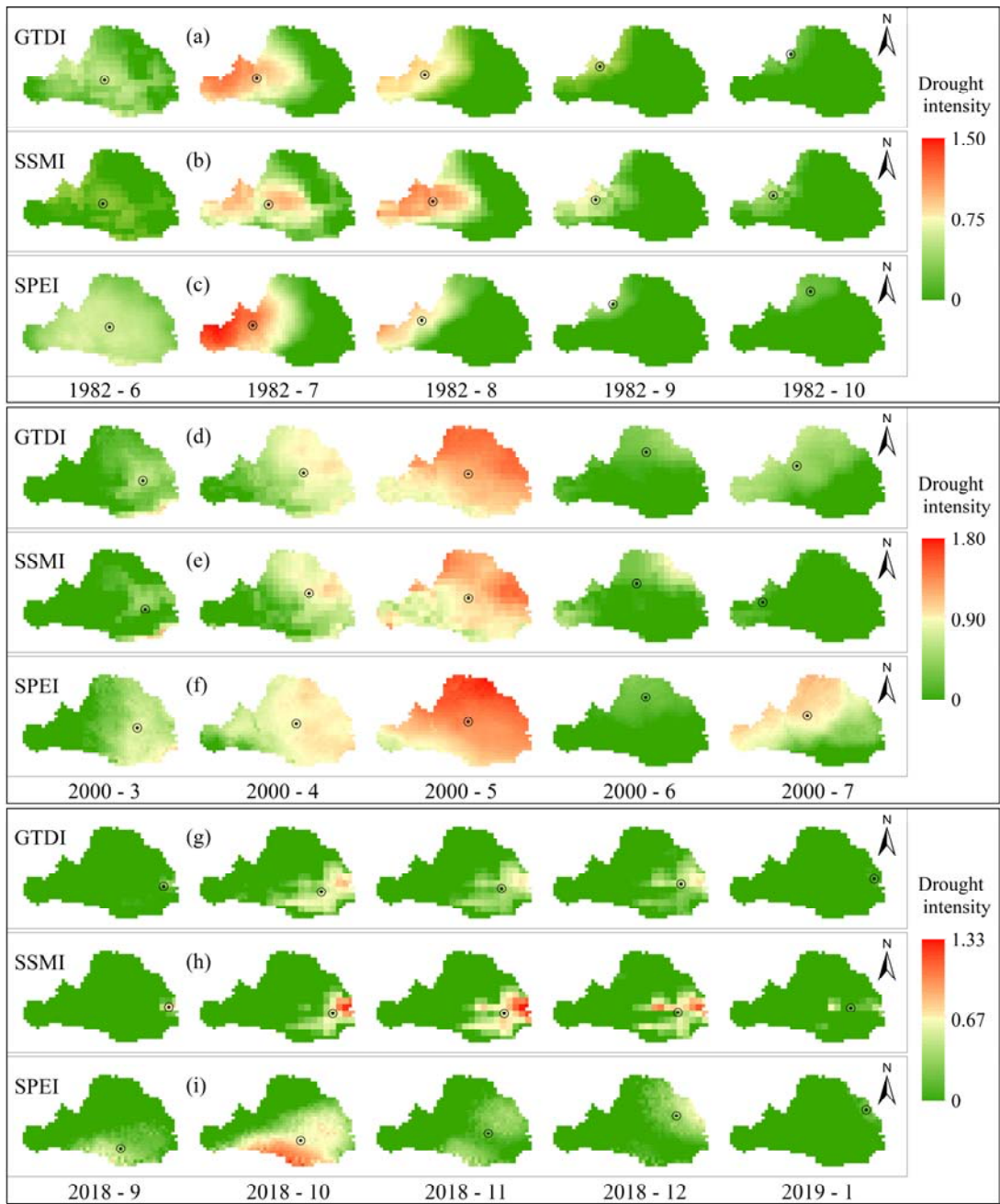
439 The above explanation suggests that using SPEI, SSMI, and GTDI for monthly-scale drought
440 identification may result in various drought trajectories. Meanwhile, the GTDI is a hybrid of the
441 hazard-causing index (SPEI) and the hazard-bearing index (SSMI), as it has a higher overlap with
442 SSMI in drought trajectory, implying changes in the hazard-bearing body during the dry period,
443 while being closer to SPEI in drought seasonal allocation, responding to the fluctuation of hazard-
444 causing factors. When paired with the GTDI index reliability analysis in Section 4.2, it is concluded
445 that the occurrence of drought events in the Wei River Basin is still dominated by precipitation
446 deficiency, ~~and~~ as the region is located in a dry location with low rainfall.

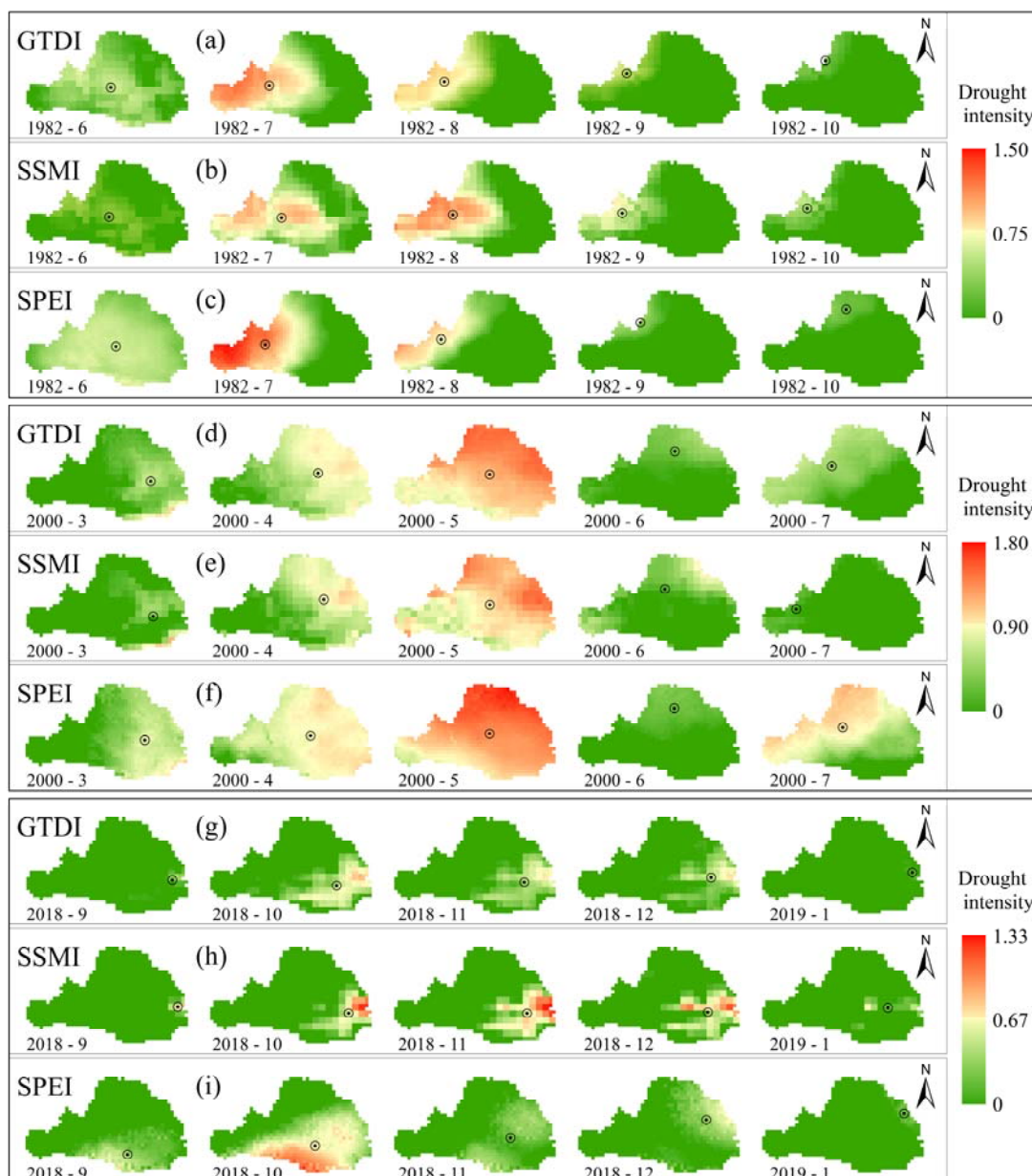
447 **4.4 Comparison of spatial evolution of drought events identified by** 448 **GTDI, SPEI, and SSMI**

449 To explore the spatial development process of drought occurrences recognized by GTDI, SPEI, and
450 SSMI while eliminating the randomness of a single event, we selected three drought events that

451 lasted for a duration of 5 months for spatial evolution analysis. Fig. 9 shows the spatial evolution
 452 processes of three drought events identified by GTDI, SPEI, and SSMI, spanning from June to
 453 October 1982, from March to July 2000, and from September 2018 to January 2019, respectively.
 454 Table 7 shows the drought intensity and the percentage of drought area for each month of the three
 455 drought events.
 456 **Table 7.** Comparison of SPEI, SSMI and GTDI in drought intensity and percentage of drought area
 457 during three drought events

Drought events	Year-month	Drought intensity			Percentage of drought area		
		SPEI	GTDI	SSMI	SPEI	GTDI	SSMI
1982	1982-6	0.47	0.31	0.28	100%	85.9%	55.7%
	1982-7	0.77	0.66	0.55	63.2%	67.0%	81.5%
	1982-8	0.52	0.57	0.71	42.5%	49.3%	58.5%
	1982-9	0.17	0.22	0.37	15.0%	23.3%	35.9%
	1982-10	0.15	0.13	0.22	17.4%	14.1%	22.4%
2000	2000-3	0.49	0.32	0.29	74.1%	61.2%	32.3%
	2000-4	0.82	0.66	0.58	98.2%	92.7%	79.3%
	2000-5	1.29	1.17	1.03	100%	100%	100%
	2000-6	0.18	0.21	0.31	38.4%	50.1%	54.3%
	2000-7	0.76	0.41	0.11	87.0%	66.6%	15.5%
2018	2018-9	0.23	0.10	0.33	35.9%	5.3%	3.0%
	2018-10	0.55	0.41	0.46	65.6%	34.2%	21.0%
	2018-11	0.20	0.31	0.55	46.5%	32.4%	28.7%
	2018-12	0.22	0.27	0.46	43.3%	31.0%	27.5%
	2019-1	0.11	0.06	0.22	5.3%	1.8%	7.5%





459

460 **Figure 9.** Comparison of SPEI, SSMI and GTDI in the spatial evolution of three drought events.

461 The black circle donates the monthly drought centroid.

462 Taking the 1982 drought event as an example, the meteorological drought emerges initially,
 463 followed by a steady decrease in its impact areas (Fig. 9c). However, the overall drought intensity
 464 increases and subsequently decreases (Table 7), and the drought centroid migrates from the WRB's
 465 center to the northwest. It is worth noting that concurrent agricultural drought lags behind
 466 meteorological drought. When comparing the drought geographic evolution processes identified by

467 SSMI and SPEI (Fig. 9b-c), the lag period is approximately one month, which is similarly observed
468 in the other two drought events (Fig. 9d-i). For the entire spatial evolution process of a drought event
469 identified by GTDI, it is clear that its spatial pattern is the result of a compromise of SPEI and SSMI,
470 including the migration path of the drought centroid (Fig. 9a-c), the evolution process of drought
471 area percentage, and drought intensity (Table 7).

472 From March to July 2000, the WRB experienced a fully covered drought event (Fig. 9d-f),
473 which began with a meteorological drought. The fusion description of SPEI and SSMI produced by
474 GTDI during this event, which incorporates the spatial evolution trends of SPEI and SSMI to
475 evaluate the current drought status at each grid point, may be observed. The value of GTDI
476 consistently falls between SPEI and SSMI, regardless of whether it is evaluated by the drought area
477 ratio, drought intensity, or drought centroid.

478 The 2018 drought event is the mildest of the three, but it most fully depicts the process of a
479 drought event from emergence to spread to eventual extinction (Fig. 9g-i). In the early stages of this
480 drought event, as of October 2018, the meteorological drought in the southeastern part of the WRB
481 was the most severe, whilst the agricultural drought was relatively negligible. In this case, the spatial
482 drought pattern determined by GTDI was closer to the development of hazard-causing index SPEI.
483 However, during the later stages of the drought event, the situation reverses and the spatial evolution
484 of drought begins to be dominated by the hazard-bearing index SSMI, illustrating GTDI possesses
485 more realistic and intelligent feature in drought identification. This also demonstrates the
486 importance of including game theory in this study, which has a distinct benefit in monitoring
487 changes in hazard-causing and bearing impacts.

488 Based on the foregoing, it is worth noting that the GTDI-identified spatial drought process

489 combines the evolutionary features of hazard-causing and bearing indices (SPEI and SSMI). ~~In~~
490 ~~addition, merging~~ SPEI and SSMI via their game relationship, rather than simply putting them
491 together, makes GTDI a superior technique to represent the spatial and temporal evolution of
492 droughts. Furthermore, it has been discovered that the GTDI exhibits the gaming feature of the
493 drought hazard-causing and bearing index. This is evidenced by the fact that the hazard-causing
494 index SPEI primarily drives the early stages of drought events in the WRB, while the hazard-bearing
495 index SSMI primarily drives the later stages.

496 **5 Conclusions**

497 This study integrated the SPEI (meteorological index and drought hazard-causing index) and SSMI
498 (agricultural index and drought hazard-bearing index) to propose a game theory-based drought index
499 (GTDI). The integration performance and weight allocation of the GTDI were demonstrated by
500 evaluating the correlations with SPEI and SSMI, and comparing the integrated weight to the ETDI
501 (entropy theory-based drought index); the reliability of the GTDI was confirmed by the Leaf Area
502 Index (LAI) data; and the advancedness of the GTDI was examined by contrasting the temporal
503 trajectories and spatial evolution characteristics of GTDI, SPEI, and SSMI. The following are the
504 primary conclusions:

505 ~~The single-type drought indices (SPEI and SSMI) and the integrated drought index (GTDI)~~
506 ~~exhibit dependable spatial consistency. In all locations within the Wei River Basin during the four~~
507 ~~seasons, there is a greatly high correlation between GTDI and SPEI. The correlation between GTDI~~
508 ~~and SSMI is relatively weak in the winter, only reaching a high correlation in 54.8% of the basin,~~
509 ~~while it continues to have exceptionally high correlations throughout the basin during the other three~~

510 seasons.

511 The entropy theory based drought index ETDI performs worse than the GTDI, particularly
512 when it comes to the regional distribution of correlation coefficient homogeneity. Specially, the
513 game theory technique provides an integrated weight geographic distribution in the integrated index
514 GTDI that is consistent with the precipitation dominated natural drought pattern. Furthermore, there
515 is a strong negative spatial relationship between the weight ratio of SPEI to SSMI and the average
516 annual precipitation in the Wei River Basin, with a correlation coefficient of -0.88. The ETDI, on
517 the other hand, has a very weak connection (correlation coefficient of -0.04) with the annual mean
518 precipitation. This indicates that the GTDI's weight distribution of SPEI and SSMI is more logical
519 and trustworthy.

520 The GTDI has superior efficacy for identifying drought when compared to the ETDI, SPEI,
521 and SSMI. When drought occurs, GTDI efficiently captures it with an efficacy ratio of over 70% in
522 all validation months, whereas ETDI, SPEI, and SSMI catch it with an efficacy ratio of
523 approximately 50%. In terms of drought impact, GTDI can capture drought occurrence in most
524 places but fails in the forest due to insufficient depth of soil surface layer measurement, whereas
525 ETDI, SPEI, and SSMI drought detection are geographically random and chaotic. Thus, GTDI is
526 expected to replace single type drought indices to provide a more accurate portrayal of actual
527 drought.

528 The GTDI merges SPEI and SSMI via their game relationship rather than simply putting them
529 together, making it a superior technique to represent the spatial and temporal evolution of droughts.
530 Due to the GTDI is a hybrid of the hazard causing index (SPEI) and the hazard bearing index
531 (SSMI), it represents diverse drought trajectories identified by the monthly scale SPEI and SSMI.

532 ~~Specially, it has a higher overlap with SSMI in drought trajectory, implying changes in the hazard-~~
533 ~~bearing body during the dry period, while being closer to SPEI in drought seasonal allocation,~~
534 ~~responding to the fluctuation of hazard causing factors. Additionally, it has been discovered that~~
535 ~~GTDI exhibits the gaming feature of the drought hazard causing and bearing index, having a distinct~~
536 ~~benefit in monitoring changes in their impacts.~~

537 ~~According to an investigation of monthly GTDI in the Wei River Basin from 1950 to 2020,~~
538 ~~there is a growing propensity for drought, particularly since the 1990s, when the intensity and~~
539 ~~frequency of drought in the WRB have increased significantly. Drought deterioration is most visible~~
540 ~~in the spring, insignificant in the summer and autumn, and most areas embrace drought reduction in~~
541 ~~the winter. Drought events in the Wei River Basin are dominated by a lack of precipitation. The~~
542 ~~hazard causing index SPEI dominates the early stages of a drought event, whereas the hazard-~~
543 ~~bearing index SSMI dominates the later stages.~~The single-type drought indices (SPEI and SSMI)
544 and the integrated drought index (GTDI) exhibit dependable spatial consistency. The entropy theory-
545 based drought index ETDI performs worse than the GTDI, particularly when it comes to the regional
546 distribution of correlation coefficient homogeneity. Specially, the game theory technique provides
547 an integrated weight geographic distribution in the integrated index GTDI that is consistent with the
548 precipitation-dominated natural drought pattern, as there is a strong negative spatial relationship
549 between the weight ratio of SPEI to SSMI and the average annual precipitation in the Wei River
550 Basin. The ETDI, on the other hand, has a very weak connection with the annual mean precipitation.
551 This indicates that the GTDI's weight allocation of SPEI and SSMI is more logical and trustworthy.

552 The GTDI has superior efficacy for identifying drought when compared to the ETDI, SPEI,
553 and SSMI, as the GTDI efficiently captures drought with an efficacy ratio of over 70% in all

554 validation months, whereas the ETDI, SPEI, and SSMI catch it with an efficacy ratio of
555 approximately 50%. Thus, GTDI is expected to replace single-type drought indices to provide a
556 more accurate portrayal of actual drought.

557 The GTDI merges SPEI and SSMI via their game relationship rather than simply putting them
558 together, making it a superior technique to represent the spatial and temporal evolution of droughts.
559 Specially, it has a higher overlap with SSMI in drought trajectory, implying changes in the hazard-
560 bearing body during the dry period, while being closer to SPEI in drought seasonal allocation,
561 responding to the fluctuation of hazard-causing factors.

562 Additionally, it has been discovered that GTDI exhibits the gaming feature of the drought
563 hazard-causing and bearing index, having a distinct benefit in monitoring changes in their impacts.
564 The hazard-causing index SPEI dominates the early stages of a drought event, whereas the hazard-
565 bearing index SSMI dominates the later stages.

566 **Acknowledgments**

567 This research is supported by the National Natural Science Foundation of China (51979005), the
568 Natural Science Basic Research Program of Shaanxi Province (2022JC-LHJJ-03) and the
569 Fundamental Research Funds for the Central Universities (300102293201). Our cordial thanks
570 should be extended to the editor and anonymous reviewers for their pertinent and professional
571 suggestions and comments which are greatly helpful for further improvement of the quality of this
572 paper.

573 Reference

- 574 Agbo, E.P., Nkajoe, U., and Edet, C.O.: Comparison of Mann–Kendall and Şen’s innovative trend
575 method for climatic parameters over Nigeria’s climatic zones, *Clim Dyn.*, 60, 3385-3401,
576 <https://doi.org/10.1007/s00382-022-06521-9>, 2023.
- 577 AghaKouchak, A., Huning, L.S., Sadegh, M., Qin, Y., Markonis, Y., Vahedifard, F., Love, C.A.,
578 Mishra, A., Mehran, A., Obringer, R., Hjelmstad, A., Pallickara, S., Jiwa, S., Hanel, M., Zhao, Y.,
579 Pendergrass, A.G., Arabi, M., Davis, S.J., Ward, P.J., Svoboda, M., Pulwarty, R., and Kreibich,
580 H.: Toward impact-based monitoring of drought and its cascading hazards, *Nat. Rev. Earth*
581 *Environ.*, 4, 582-595, <https://doi.org/10.1038/s43017-023-00457-2>, 2023.
- 582 Bai, Y., Liu, M., Guo, Q., Wu, G., Wang, W., and Li, S.: Diverse responses of gross primary
583 production and leaf area index to drought on the Mongolian Plateau, *Sci. Total Environ.*, 902,
584 166507, <https://doi.org/10.1016/j.scitotenv.2023.166507>, 2023.
- 585 Batabyal, A.A. and Beladi, H.: A game-theoretic model of water theft during a drought, *Agric. Water*
586 *Manage.*, 255, 107044, <https://doi.org/10.1016/j.agwat.2021.107044>, 2021.
- 587 Berg, A. and Sheffield, J.: Climate change and drought: the soil moisture perspective, *Curr. Clim.*
588 *Chang. Rep.*, 4, 180-191, <https://doi.org/10.1007/s40641-018-0095-0>, 2018.
- 589 [Blauhut, V., Stahl, K., Stagge, J. H., Tallaksen, L. M., De Stefano, L., and Vogt, J.: Estimating](https://doi.org/10.5194/hess-20-2779-2016)
590 [drought risk across Europe from reported drought impacts, drought indices, and vulnerability](https://doi.org/10.5194/hess-20-2779-2016)
591 [factors. *Hydrol. Earth Syst. Sci.*, 20, 2779–2800, <https://doi.org/10.5194/hess-20-2779-2016>,](https://doi.org/10.5194/hess-20-2779-2016)
592 [2016.](https://doi.org/10.5194/hess-20-2779-2016)
- 593 Bock, A.D., Belmans, B., Vanlanduit, S., Blom, J., Alvarado-Alvarado, A.A., and Audenaert, A.: A
594 review on the leaf area index (LAI) in vertical greening systems, *Build. Environ.*, 229, 109926,

595 <https://doi.org/10.1016/j.buildenv.2022.109926>, 2023.

596 Cai, Y., Zhang, F., Duan, P., Jim, C.Y., Chan, N.W., Shi, J., Liu, C., Wang, J., Bahtebay, J., and Ma,
597 X.: Vegetation cover changes in China induced by ecological restoration-protection projects and
598 land-use changes from 2000 to 2020, *Catena.*, 217, 106530,
599 <https://doi.org/10.1016/j.catena.2022.106530>, 2022.

600 Chang, J., Li, Y., Wang, Y., and Yuan, M.: Copula-based drought risk assessment combined with an
601 integrated index in the Wei River Basin, China, *J. Hydrol.*, 540, 824-834,
602 <https://doi.org/10.1016/j.jhydrol.2016.06.064>, 2016.

603 Chen, Q., Timmermans, J., Wen, W., and van Bodegom, P.M.: A multi-metric assessment of drought
604 vulnerability across different vegetation types using high resolution remote sensing, *Sci. Total*
605 *Environ.*, 832, 154970, <https://doi.org/10.1016/j.scitotenv.2022.154970>, 2022.

606 Dai, A.: Drought under global warming: a review, *Wiley Interdiscipl. Rev. Clim. Change.*, 2, 45-65,
607 <https://doi.org/10.1002/wcc.81>, 2011.

608 Dai, A.: Increasing drought under global warming in observations and models, *Nat. Clim. Change.*,
609 3, 52-58, <https://doi.org/10.1038/nclimate1633>, 2013.

610 Deng, C.L., She, D.X., Zhang, L.P., Zhang, Q., Liu, X., and Wang, S.X.: Characteristics of drought
611 events using three-dimensional graph connectedness recognition method in the Yangtze River
612 Basin, China, *Trans. Chin. Soc. Agric. Eng.*, 37, 131-139, 2021.

613 Ding, Y., Gong, X., Xing, Z., Cai, H., Zhou, Z., Zhang, D., Sun, P., and Shi, H.: Attribution of
614 meteorological, hydrological and agricultural drought propagation in different climatic regions of
615 China, *Agric. Water Manage.*, 255, 106996, <https://doi.org/10.1016/j.agwat.2021.106996>, 2021.

616 Fang, H., Baret, F., Plummer, S., and Schaepman-Strub, G.: An overview of global leaf area index

617 (LAI): Methods, products, validation, and applications, *Rev. Geophys.*, 57, 739-799,
618 <https://doi.org/10.1029/2018RG000608>, 2019.

619 Feng, K., Yan, Z., Li, Y., Wang, F., Zhang, Z., Su, X., Wu, H., Zhang, G., and Wang, Y.: Spatio-
620 temporal dynamic evaluation of agricultural drought based on a three-dimensional identification
621 method in Northwest China, *Agric. Water Manage.*, 284, 108325,
622 <https://doi.org/10.1016/j.agwat.2023.108325>, 2023.

623 Hao, Z. and AghaKouchak, A.: Multivariate standardized drought index: a parametric multi-index
624 model, *Adv. Water Resour.*, 57, 12-18, <https://doi.org/10.1016/j.advwatres.2013.03.009>, 2013.

625 [Huang, F., Liu, L., Gao, J., Yin, Z., Zhang, Y., Jiang, Y., and Fang, W.: Effects of extreme drought](https://doi.org/10.1016/j.scitotenv.2023.166562)
626 [events on vegetation activity from the perspectives of meteorological and soil droughts in](https://doi.org/10.1016/j.scitotenv.2023.166562)
627 [southwestern China. *Sci. Total Environ.*, 903, 166562, 2023.](https://doi.org/10.1016/j.scitotenv.2023.166562)

628 Huang, J., Yu, H., Guan, X., Wang, G., and Guo, R.: Accelerated dryland expansion under climate
629 change, *Nat. Clim. Chang.*, 6, 166-171, <https://doi.org/10.1038/nclimate2837>, 2016.

630 Huang, S., Chang, J., Leng, G., and Huang, Q.: Integrated index for drought assessment based on
631 variable fuzzy set theory: a case study in the Yellow River basin, China, *J. Hydrol.*, 527, 608-618,
632 <https://doi.org/10.1016/j.jhydrol.2015.05.032>, 2015.

633 Jato-Espino, D. and Ruiz-Puente, C.: Bringing Facilitated Industrial Symbiosis and Game Theory
634 together to strengthen waste exchange in industrial parks, *Sci. Total Environ.*, 771, 145400,
635 <https://doi.org/10.1016/j.scitotenv.2021.145400>, 2021.

636 Jiang, W., Wang, L., Feng, L., Zhang, M., and Yao, R.: Drought characteristics and its impact on
637 changes in surface vegetation from 1981 to 2015 in the Yangtze River Basin, China, *Int. J.*
638 *Climatol.*, 40, 3380-3397, <https://doi.org/10.1002/joc.6403>, 2020.

639 Khorshidi, M.S., Nikoo, M.R., Sadegh, M., and Nematollahi, B.: A multi-objective risk-based game
640 theoretic approach to reservoir operation policy in potential future drought condition, *Water*
641 *Resour. Manage.*, 33, 1999-2014, <https://doi.org/10.1007/s11269-019-02223-w>, 2019.

642 Labudová, L., Labuda, M., and Takáč, J.: Comparison of SPI and SPEI applicability for drought
643 impact assessment on crop production in the Danubian Lowland and the East Slovakian Lowland,
644 *Theor. Appl. Climatol.*, 128, 491-506, <https://doi.org/10.1007/s00704-016-1870-2>, 2017.

645 Lai, C., Chen, X., Chen, X., Chen, X., Wang, Z., Wu, X., and Zhao, S.: A fuzzy comprehensive
646 evaluation model for flood risk based on the combination weight of game theory, *Nat. Hazards.*,
647 77, 1243-1259, <https://doi.org/10.1007/s11069-015-1645-6>, 2015.

648 Leng, G., Tang, Q., and Rayburg, S.: Climate change impacts on meteorological, agricultural and
649 hydrological droughts in China, *Glob. Planet. Chang.*, 126, 23-34,
650 <https://doi.org/10.1016/j.gloplacha.2015.01.003>, 2015.

651 Li, G., Sun, S., Han, J., Yan, J., Liu, W., Wei, Y., Lu, N., and Sun, Y.: Impacts of Chinese Grain for
652 Green program and climate change on vegetation in the Loess Plateau during 1982–2015, *Sci.*
653 *Total Environ.*, 660, 177-187, <https://doi.org/10.1016/j.scitotenv.2019.01.028>, 2019.

654 Li, L., She, D., Zheng, H., Lin, P., and Yang, Z.: Elucidating diverse drought characteristics from
655 two meteorological drought indices (SPI and SPEI) in China, *J. Hydrometeorol.*, 21, 1513-1530,
656 <https://doi.org/10.1175/JHM-D-19-0290.1>, 2020.

657 Li, W., Migliavacca, M., Forkel, M., Denissen, J.M.C., Reichstein, M., Yang, H., Duveiller, G.,
658 Weber, U., and Orth, R.: Widespread increasing vegetation sensitivity to soil moisture, *Nat.*
659 *Commun.*, 13, 3959, <https://doi.org/10.1038/s41467-022-31667-9>, 2022.

660 Liu, B., Huang, J.J., McBean, E., and Li, Y.: Risk assessment of hybrid rain harvesting system and

661 other small drinking water supply systems by game theory and fuzzy logic modeling, *Sci. Total*
662 *Environ.*, 708, 134436, <https://doi.org/10.1016/j.scitotenv.2019.134436>, 2020.

663 [Liu, Y., Liu, R., and Chen, J.M.: Retrospective retrieval of long-term consistent global leaf area](#)
664 [index \(1981–2011\) from combined AVHRR and MODIS data, *J. Geophys. Res.*, 117, G04003,](#)
665 <https://doi.org/10.1029/2012JG002084>, 2012.

666 Liu, Y., Zhu, Y., Ren, L., Yong, B., Singh, V.P., Yuan, F., Jiang, S., and Yang, X.: On the mechanisms
667 of two composite methods for construction of multivariate drought indices, *Sci. Total Environ.*,
668 647, 981-991, <https://doi.org/10.1016/j.scitotenv.2018.07.273>, 2019.

669 Ma, B., Zhang, B., Jia, L., and Huang, H.: Conditional distribution selection for SPEI-daily and its
670 revealed meteorological drought characteristics in China from 1961 to 2017, *Atmos. Res.*, 246,
671 105108, <https://doi.org/10.1016/j.atmosres.2020.105108>, 2020.

672 Madani, K.: Game theory and water resources, *J. Hydrol.*, 381, 225-238,
673 <https://doi.org/10.1016/j.jhydrol.2009.11.045>, 2010.

674 McKee, T.B., Doesken, N.J., and Kleist, J.: The relationship of drought frequency and duration to
675 time scales, Paper Presented at Proceedings of the 8th Conference on Applied Climatology, 17,
676 179-183, 2010.

677 Ministry of Water Resources of China: China Flood and Drought Disaster Prevention Bulletin,
678 China Water Power Press, Beijing, 2022.

679 Oertel, M., Meza, F.J., Gironás, J., Scott, C.A., Rojas, F., and Pineda-Pablos, N.: Drought
680 propagation in semi-arid river basins in Latin America: lessons from Mexico to the Southern Cone,
681 *Water*, 10, 1564, <https://doi.org/10.3390/w10111564>, 2018.

682 Palmer, W.C.: Meteorological drought, US Department of Commerce, Weather Bureau, Washington,

683 DC, 1965.

684 [Panda, P.K., Panda, R.B., and Dash, P.K.: The study of water quality and pearson's correlation](#)
685 [coefficients among different physico-chemical parameters of River Salandi, Bhadrak, Odisha,](#)
686 [India. Am. J. Water Resour., 6, 146-155, 2018.](#)

687 [Peng, S., Ding, Y., Liu, W., and Li, Z.: 1 km monthly temperature and precipitation dataset for China](#)
688 [from 1901 to 2017, Earth Syst. Sci. Data, 11, 1931–1946, \[https://doi.org/10.5194/essd-11-1931-\]\(https://doi.org/10.5194/essd-11-1931-2019\)](#)
689 [2019, 2019.](#)

690 Saha, A., Pal, S.C., Chowdhuri, I., Roy, P., Chakraborty, R., and Shit, M.: Vulnerability assessment
691 of drought in India: Insights from meteorological, hydrological, agricultural and socio-economic
692 perspectives, Gondw. Res., 123, 68-88, <https://doi.org/10.1016/j.gr.2022.11.006>, 2023.

693 Shah, D., and Mishra, V.: Integrated Drought Index (IDI) for drought monitoring and assessment in
694 India, Water Resour. Res., 56, e2019WR026284, <https://doi.org/10.1029/2019WR026284>, 2020.

695 Shukla, S., and Wood, A.W.: Use of a standardized runoff index for characterizing hydrologic
696 drought, Geophys. Res. Lett., 35, <https://doi.org/10.1029/2007GL032487>, 2008.

697 Tan, Y.X., Ng, J.L., and Huang, Y.F.: Quantitative analysis of input data uncertainty for SPI and
698 SPEI in Peninsular Malaysia based on the bootstrap method, Hydrol. Sci. J., 68, 1724-1737,
699 <https://doi.org/10.1080/02626667.2023.2232348>, 2023.

700 Tian, P., Liu, L., Tian, X., Zhao, G., Klik, A., Wang, R., Lu, X., Mu, X., and Bai, Y.: Sediment yields
701 variation and response to the controlling factors in the Wei River Basin, China, Catena., 213,
702 106181, <https://doi.org/10.1016/j.catena.2022.106181>, 2022.

703 Trenberth, K.E., Dai, A., Van, and van der Schrier, G.: Global warming and changes in drought, Nat.
704 Clim. Change., 4, 17-22, <https://doi.org/10.1038/nclimate2067>, 2014.

705 Vicente-Serrano, S.M., Beguería, S., and López-Moreno, J.I.: A multiscalar drought index sensitive
706 to global warming: the standardized precipitation evapotranspiration index, *J. Clim.*, 23, 1696-
707 1718, <https://doi.org/10.1175/2009JCLI2909.1>, 2010.

708 Vicente-Serrano, S.M., Quiring, S.M., Pena-Gallardo, M., Yuan, S., and Domínguez-Castro, F.: A
709 review of environmental droughts: Increased risk under global warming? *Earth Sci. Rev.*, 201,
710 102953, <https://doi.org/10.1016/j.earscirev.2019.102953>, 2020.

711 Wang, A., Lettenmaier, D.P., and Sheffield, J.: Soil moisture drought in China, 1950–2006, *J. Clim.*,
712 24, 3257-3271, <https://doi.org/10.1175/2011JCLI3733.1>, 2011.

713 Wang, F., Wang, Z., Yang, H., Di, D., Zhao, Y., Liang, Q., and Hussain, Z.: Comprehensive
714 evaluation of hydrological drought and its relationships with meteorological drought in the
715 Yellow River basin, China, *J. Hydrol.*, 584, 124751,
716 <https://doi.org/10.1016/j.jhydrol.2020.124751>, 2020.

717 Wang, X., Luo, P., Zheng, Y., Duan, W., Wang, S., Zhu, W., Zhang, Y., and Nover, D.: Drought
718 Disasters in China from 1991 to 2018: Analysis of Spatiotemporal Trends and Characteristics,
719 *Remote Sens.*, 15, 1708, <https://doi.org/10.3390/rs15061708>, 2023.

720 Wang, Z., Zhong, R., Lai, C., Zeng, Z., Lian, Y., and Bai, X.: Climate change enhances the severity
721 and variability of drought in the Pearl River Basin in South China in the 21st century, *Agric. For.*
722 *Meteorol.*, 249, 149-162, <https://doi.org/10.1016/j.agrformet.2017.12.077>, 2018.

723 Wei, H., Liu, X., Hua, W., Zhang, W., Ji, C., and Han, S.: Copula-Based Joint Drought Index Using
724 Precipitation, NDVI, and Runoff and Its Application in the Yangtze River Basin, China, *Remote*
725 *Sens.*, 15, 4484, <https://doi.org/10.3390/rs15184484>, 2023.

726 Wen, X., Tu, Y., Tan, Q., Li, W., Fang, G., Ding, Z., and Wang, Z.: Construction of 3D drought

727 structures of meteorological drought events and their spatio-temporal evolution characteristics, J.
728 Hydrol., 590, 125539, <https://doi.org/10.1016/j.jhydrol.2020.125539>, 2020.

729 Wilhite, D.A., and Glantz, M.H.: Understanding: the drought phenomenon: the role of definitions,
730 Water Int., 10, 111-120, 1985.

731 Won J, Choi J, Lee O, and Kim, S.: Copula-based Joint Drought Index using SPI and EDDI and its
732 application to climate change, Sci. Total Environ., 744, 140701,
733 <https://doi.org/10.1016/j.scitotenv.2020.140701>, 2020.

734 Xu, H., Wang, X., Zhao, C., and Yang, X.: Diverse responses of vegetation growth to meteorological
735 drought across climate zones and land biomes in northern China from 1981 to 2014, Agric. For.
736 Meteorol., 262, 1-13, <https://doi.org/10.1016/j.agrformet.2018.06.027>, 2018.

737 Xu, Y., Zhang, X., Hao, Z., Singh, V.P., and Hao, F.: Characterization of agricultural drought
738 propagation over China based on bivariate probabilistic quantification, J. Hydrol., 598, 126194,
739 <https://doi.org/10.1016/j.jhydrol.2021.126194>, 2021.

740 Xu, Y., Zhang, X., Wang, X., Hao, Z., Singh, V.P., and Hao, F.: Propagation from meteorological
741 drought to hydrological drought under the impact of human activities: A case study in northern
742 China, J. Hydrol., 579, 124147, <https://doi.org/10.1016/j.jhydrol.2019.124147>, 2019.

743 [Yang, Y., and He, Y.: A fault identification method based on an ensemble deep neural network and](https://doi.org/10.1016/j.softcom.2022.107343)
744 [a correlation coefficient. Soft Comput., 26, 9199-9214, https://doi.org/10.1007/s00500-022-](https://doi.org/10.1016/j.softcom.2022.107343)
745 [07343-x, 2022.](https://doi.org/10.1007/s00500-022-107343-x)

746 Yang, J., Gong, D., Wang, W., Hu, M., and Mao, R.: Extreme drought event of 2009/2010 over
747 southwestern China, Meteorol. Atmos. Phys., 115, 173-184, [https://doi.org/10.1007/s00703-011-](https://doi.org/10.1007/s00703-011-0172-6)
748 [0172-6](https://doi.org/10.1007/s00703-011-0172-6), 2012.

749 You, M., He, Z.H., Zhang, L., Yang, M.K., and Pi, G.N.: Characteristics of agricultural and
750 meteorological drought in Guizhou Province and their response relationship, *J. Soil Water*
751 *Conserv.*, 36, 255-264, 2022.

752 [Yue, S., and Wang, C.Y.: Applicability of prewhitening to eliminate the influence of serial](#)
753 [correlation on the Mann-Kendall test. *Water Resour. Res.*, 38, 4-1-4-7,](#)
754 <https://doi.org/10.1029/2001WR000861>, 2002.

755 Zhang, F., Biederman, J.A., Dannenberg, M.P., Yan, D., Reed, S.C., and Smith, W.K.: Five decades
756 of observed daily precipitation reveal longer and more variable drought events across much of
757 the western United States, *Geophys. Res. Lett.*, 48, e2020GL092293,
758 <https://doi.org/10.1029/2020GL092293>, 2021.

759 Zhang, J., Wang, J., Chen, S., Wang, M., Tang, S., and Zhao, W.: Integrated Risk Assessment of
760 Agricultural Drought Disasters in the Major Grain-Producing Areas of Jilin Province, China,
761 *Land.*, 12, 160, <https://doi.org/10.3390/land12010160>, 2023.

762 Zhang, T., Su, X., Zhang, G., Wu, H., Wang, G., and Chu, J.: Evaluation of the impacts of human
763 activities on propagation from meteorological drought to hydrological drought in the Weihe River
764 Basin, China, *Sci. Total Environ.*, 819, 153030, <https://doi.org/10.1016/j.scitotenv.2022.153030>,
765 2022.

766 [Zhang, Q., Shi, R., Singh, V.P., Xu, C., Yu, H., Fan, K., and Wu, Z.: Droughts across China: Drought](#)
767 [factors, prediction and impacts. *Sci. Total Environ.*, 803, 150018,](#)
768 <https://doi.org/10.1016/j.scitotenv.2021.150018>, 2022.

769 Zhang, X., Hao, Z., Singh, V.P., Zhang, Y., Feng, S., Xu, Y., and Hao, F.: Drought propagation under
770 global warming: Characteristics, approaches, processes, and controlling factors, *Sci. Total*

771 Environ., 838, 156021, <https://doi.org/10.1016/j.scitotenv.2022.156021>, 2022.

772 Zhang, Y., Hao, Z., Feng, S., Zhang, X., Xu, Y., and Hao, F.: Agricultural drought prediction in
773 China based on drought propagation and large-scale drivers, *Agric. Water Manage.*, 255, 107028,
774 <https://doi.org/10.1016/j.agwat.2021.107028>, 2021.

775 Zhang, Y., Huang, S., Huang, Q., Leng, G., Wang, H., and Wang, L.: Assessment of drought
776 evolution characteristics based on a nonparametric and trivariate integrated drought index, *J.*
777 *Hydrol.*, 579, 124230, <https://doi.org/10.1016/j.jhydrol.2019.124230>, 2019.

778